CHAPTER 3

ANALYSIS OF THE INTERFACE BEHAVIOR IN PURE SHEAR SPECIMENS BY MEANS OF NON-LINEAR FRACTURE MECHANICS (NLFM)

3.1. Introduction to Non-Linear Fracture Mechanics

The transfer of stresses from concrete to FRP is a crucial fact on the correct performance of externally reinforced concrete structures. Failures in this transfer region may result in brittle ruptures that must be taken into account in the design of the reinforcement. The application of Fracture Mechanics theory in this area is a useful tool to model the behavior of the interface and its premature failure.

Fracture mechanics is concerned with the description of the mechanics phenomena involving the propagation of a crack in a continuous medium. Its origins go back to the work of Griffith which was published in 1920 (Anderson, 1991). Griffith applied the stress analysis of an elliptical hole to the unstable propagation of a crack. The mechanics of fracture progressed from being a scientific curiosity to an engineering discipline during World War II because of the brittle fracture of the Liberty ships, which were the first to have an all-welded hull. In 1956, Irwin developed the energy release rate concept, which was related to the Griffith theory, but in a more useful form for solving engineering problems. Crack plasticity turned out to be an important concern around 1960. Fracture mechanics today is a well-established theory as documented for example in Anderson (1991).

Before starting with the implementation of Fracture Mechanics in the bond transfer between concrete and the external reinforcement, some fracture mechanics concepts will be introduced.

Linear Elastic Fracture Mechanics (LEFM) can be defined as the mechanical process that develops during the formation of a crack without activating plastic mechanisms. Within this process the material behaves in a linear elastic manner. LEFM applies to elastic brittle materials (i.e. glass). Two approaches can be used to describe the propagation of a crack. In the stress approach, assuming an existing crack, the theory of elasticity gives the stress distribution at the vicinity of the crack tip as equation (3.1). Fracture will occur when k reaches a characteristic value k_C, known as fracture toughness.

$$\sigma(x) = \frac{k}{\sqrt{x}} \tag{3.1}$$

where:

k: stress intensity factor

Alternatively, in the energy approach, if an existing crack with length a increases its length in a differential da, the amount of internal strain energy will vary as shown by equation (3.2).

$$\frac{\partial U}{\partial a} da = -G da \tag{3.2}$$

The energy required to grow an existing crack a total of da is given as (3.3).

$$\frac{\partial W}{\partial a} da = G_C da \tag{3.3}$$

The propagation of a crack is possible if the energy in the system decreases during the fictive extension, in other words, if equation (3.4) is accomplished:

$$G \geq G_C \tag{3.4}$$

In 1957, Irwin (Oller, S., 2001) introduced an identification of the different crack propagation movements which were categorized in three groups, as shown in Figure 3.1:

Opening mode I: The crack surfaces split up almost parallel to each other and the displacements of these points are perpendicular to the crack plane. It is assumed that only tensile stresses develop in this mode of fracture.

Shearing mode II: The crack surfaces slide between each other in the crack plane. It is assumed that only shear stresses are generated under mode II.

Tearing mode III: The crack surfaces slide laterally between each other. In this case, only shear stresses can be developed.

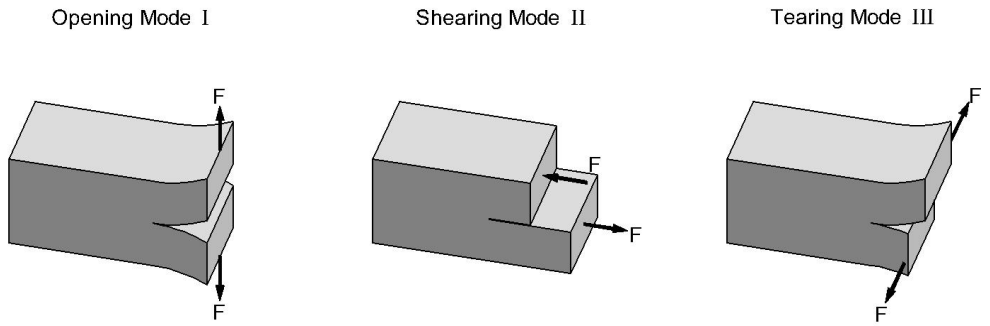

Figure 3.1. Fracture modes (adapted from Irwin, 1957).

The joints of interest here are loaded primarily in shear providing the necessary shear connection between the concrete and the FRP. The interfacial shear stresses generate a relative displacement between both adherents that may derive in the formation of a horizontal crack along the interface. Hence, the crack propagation mode will resemble Shearing mode II.

3.1.1. Application to bonded plates. Non-Linear Fracture Mechanics.

The fracture is non-linear, when plasticity or another inelastic mechanism that implies big deformations before failure, occurs on the crack tip. Therefore, Linear Elastic Fracture Mechanics (LEFM) cannot be used in ductile materials (with a pronounced yield zone) or in deformation softening materials (that have a pronounced descending branch on the load deflection curve). The last group of materials (i.e. concrete) is of interest in this work. In this case, a special Non-Linear Fracture Mechanics (NLFM) must be developed based on a stress-displacement relationship.

One aim of this research (see Figure 3.2) is the analysis of a bonded joint between a linear elastic laminate and a linear elastic support through an intermediate adhesive.

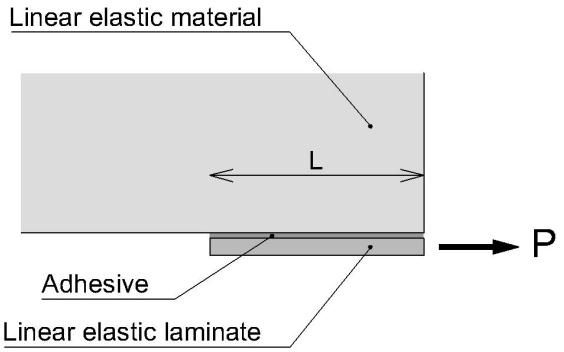

Figure 3.2. Bonded joint between a linear elastic laminate and a linear elastic support.

The debonding process of a laminate can be analyzed as the formation and propagation of an interfacial crack. The bond line is assumed as a pure shear medium. The shear stresses which are locally transferred between the concrete and the external reinforcement are related to the relative displacement between both materials through the constitutive behavior of the interface using a bond-slip function.

In Figure 3.3, some shear-slip relations for different types of reinforcement are shown. The bond of FRP is stiffer than that of embedded steel rebars, but the total load capacity of the FRP bond, which is proportional to the area under the curve, is much lower.

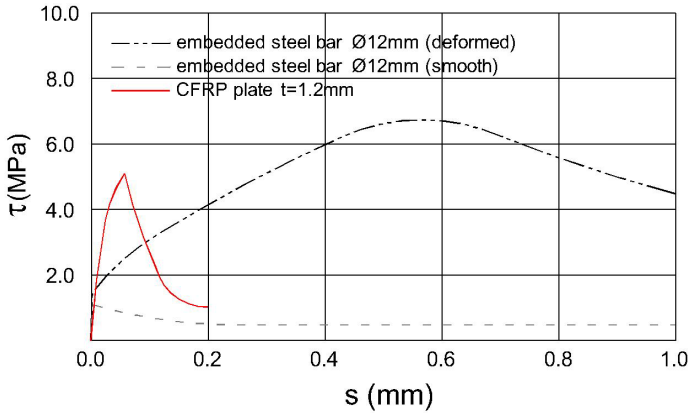

Figure 3.3. Shear stress-slip relations for different types of reinforcement (FIB Task Group 9.3 FRP, 2001).

Figure 3.4 shows a typical bond-slip relationship for a bonded joint. In this bond-slip curve, two zones are distinguished:

1) While the slip is lower than the value s_{LM}, the shear stress is a growing function representing the adhesive deformation. The joint is in Zone I. The maximum shear stress at a slip value of s_{LM} is τ_{LM}.
2) For slip values higher than s_{LM}, the shear stress is a decreasing function that reproduces the post-peak behavior. The joint is in Zone II. While in Zone I, the material is assumed to be undamaged, in Zone II, microcracks develop in the joint. Shear stress transfer is still possible by aggregate interlock. The function is valid up to a slip value of s_{L0}. At this point, the joint is assumed to be locally broken with the opening of an interfacial macrocrack.

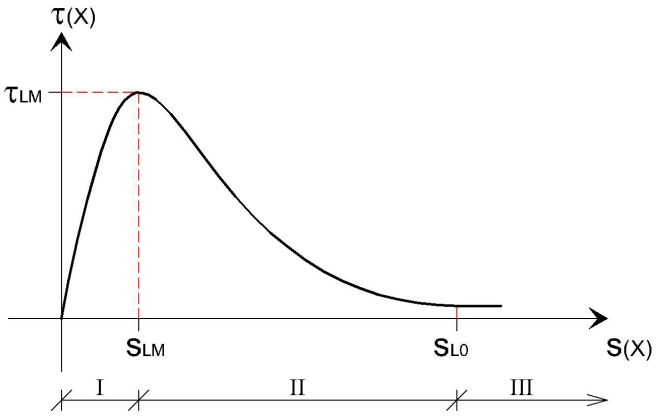

Figure 3.4. Bond-slip relationship.

The area enclosed by the bond-slip relationship up to a particular slip value, s_L, is the strain energy stored in a joint (per unit bonded area), (see Figure 3.5). When a crack opens, the store energy is released. At this point, the energy release, which is the area under the curve of Figure 3.6, is called fracture energy G_F (per unit bonded area). The fracture energy is defined as the energy required to bring to a complete fracture a connection with a certain area.

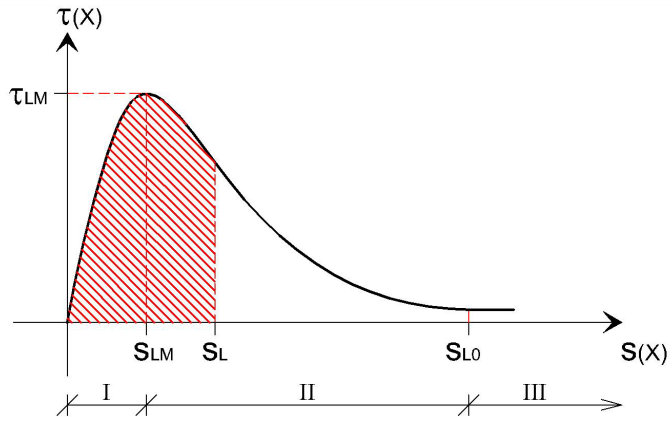

Figure 3.5. Stored energy in a joint.

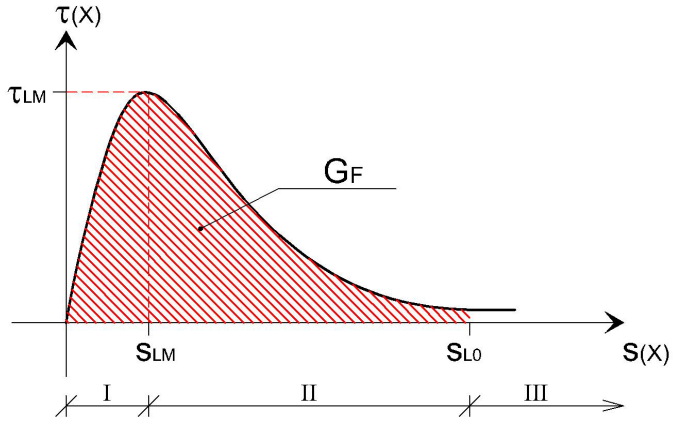

Figure 3.6. Fracture energy G_F.

Looking back to Figure 3.2, the external work done by a particular force value P will be stored as strain energy in the laminate, in the support and in the joint. Fracture growth is caused by a critical value of the applied force P_{max} that generates a strain energy release (fracture energy) compatible with an equal energy increase in the laminate.

For the particular case of a very long laminate, this maximum force P_{max} is easily obtained as follows.

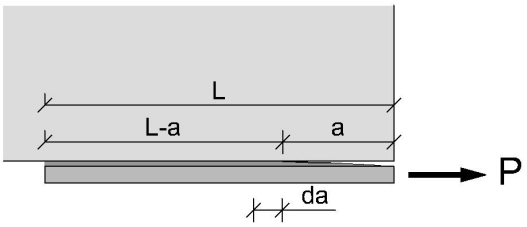

Figure 3.7. Fracture growth.

If the crack grows a differential length *da*, the stored energy in the laminate will vary by a certain amount given by equation (3.5) since it can be assumed that the laminate is substantially long and the strain stored in the bonded part of the laminate does not depend on its length.

$$dU_L = dU_{L,a} + dU_{L,l-a} = \frac{1}{2}\frac{P^2}{E_L t_L b_L} da + 0 \tag{3.5}$$

The energy release, when the fracture increases a differential *da*, is written as (3.6).

$$dW = G_F b_L da \tag{3.6}$$

Thus, fracture growth is possible when the energy release equals the stored energy, as shown in equation (3.7). From this equation, the maximum applied force is obtained (see equation (3.8)).

$$G_F b_L da = \frac{1}{2}\frac{P^2}{E_L t_L b_L} da \tag{3.7}$$

$$P_{\max} = b_L \sqrt{2 G_F E_L t_L} \tag{3.8}$$

This analysis has been based mainly on the work of Täljsten (1994). It has the advantage of being very simple, intuitive, and theoretically more accurate in describing the physics of the FRP debonding. In addition, it does not depend on the shape of the bond-slip relationship. However, it does not give a clear idea of which is the process involved in the formation and propagation of a crack. Furthermore, it is difficult to extend it to finite length laminates.

Therefore, in order to describe the crack propagation process, a strength approach (rather than an energy approach) will be presented for a bilinear bond-slip relationship in this chapter.

3.2. Governing equations

3.2.1. The Volkersen equation

In order to describe the stress and strain distribution on the interface between the support and the laminate on a beam under transverse load, it is necessary to deal with a simplified case. To avoid the presence of interface normal stresses, a pure shear case is first studied (see Figure 3.8).

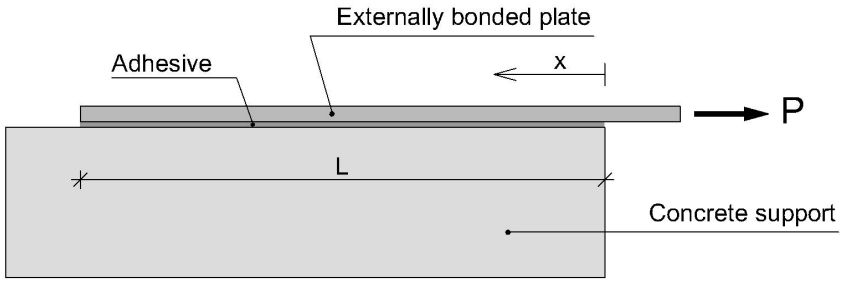

Figure 3.8. Single shear test model.

The governing equation describing the stress situation in a bonded connection can be derived using the following assumptions:

1) The adhesive is only exposed to shear forces.
2) The thickness and width of the adherents and adhesive are constant along the bonded length.
3) The bending effects in both adherents are not considered.
4) Since the concrete axial stiffness is much higher than the laminate axial stiffness, the concrete axial strain is neglected.
5) The normal stresses are uniformly distributed along the laminate cross-section.

Figure 3.9 shows a differential element, *dx*, of a bonded joint. Applying equilibrium to this element, the laminate tensile stress, σ_L, can be obtained through the shear stresses as shown in equation (3.9).

$$\tau(x) = t_L \frac{d\sigma_L}{dx}(x) \tag{3.9}$$

The relative displacement of the laminate with respect to the support will be called here laminate slip, *s*. As the concrete axial strain is neglected, the first derivative of the slip becomes equal to the laminate strain, which can be expressed as a function of the tensile stress.

$$\frac{ds(x)}{dx} = \varepsilon_L(x) = \frac{\sigma_L(x)}{E_L} \tag{3.10}$$

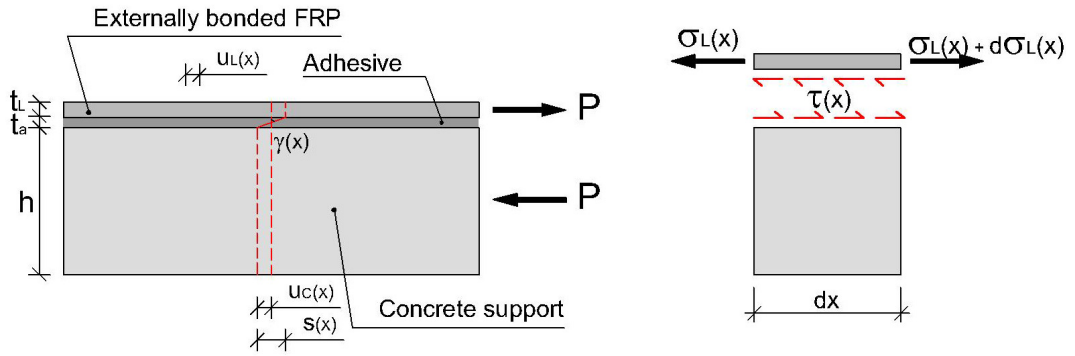

Figure 3.9. Bonded joint loaded in pure shear.

By incorporating equation (3.9) in the derivative of equation (3.10), the governing equation (3.11) can be written. This equation is expressed in terms of the relative displacement (or slip) between support and external reinforcement as represented by s and the shear stress which is a function of the slip, $\tau = f(s)$.

$$\frac{d^2 s(x)}{dx^2} - \frac{1}{E_L t_L}\tau(x) = 0 \tag{3.11}$$

The second order differential equation (3.11) describing the behavior of a bonded joint was first derived by Volkersen in 1938 (referenced by Brosens, 2001). Later on, this differential equation was used by many other researchers including Bresson (1971), Kaisser (1989) (referenced by Meier, 1995), Täljsten (1994) and Brosens (2001). Equation (3.11) can be solved by assuming a constitutive relationship between the shear stress and the slip, $\tau = f(s)$. This equation, which was originally proposed for a linear elastic stress-deformation relationship, can also be extended to any other non-linear relationship through Non-Linear Fracture Mechanics theory (NLFM).

3.2.2. Bond-slip relationship

From all the different shapes of the bond-slip curves, it has been justified (Brosens, 2001) that a bilinear function (see Figure 3.10) corresponds better with experimental data than a linear or an elasto-plastic function (see Figure 3.3). The linear approach only agrees with reality when describing the pre-peak behavior before the maximum stress is reached. The elasto-plastic function is less appropriate for brittle materials.

This bilinear bond-slip relationship can be mathematically expressed as equation (3.12):

$$s(x) = \begin{cases} \dfrac{s_{LM}}{\tau_{LM}}\tau(x) & (Zone\ I) \\ s_{LM} + \dfrac{s_{L0} - s_{LM}}{\tau_{LM}}\left(\tau_{LM} - \tau(x)\right) & (Zone\ II) \end{cases} \tag{3.12}$$

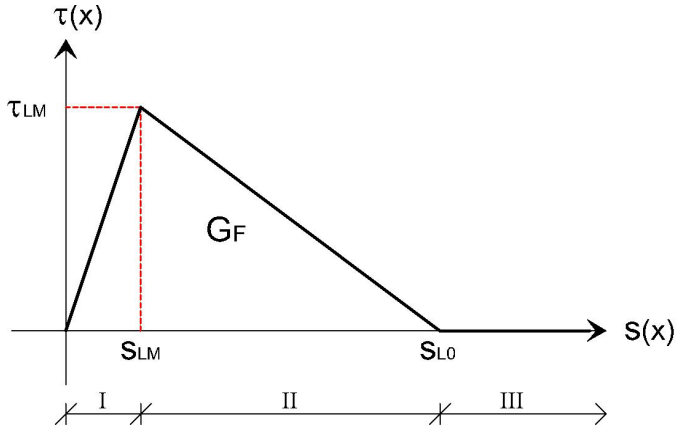

Figure 3.10. Bilinear bond – slip relationship.

When assuming a bilinear shear stress vs. relative displacement relationship, the total fracture energy, G_F, can be divided into two terms: G_F^I which is the area under the upward branch of the bond-slip relationship, and G_F^{II} which is the area enclosed by the downward branch of the τ - s curve.

$$G_F = G_F^{\ I} + G_F^{\ II} \tag{3.13}$$

As will be explained later, the slip associated to the maximum shear stress s_{LM} is always much lower than the maximum slip s_{L0}. Therefore the G_F^I component is much lower than the G_F^{II}. For instance, the total fracture energy for the laminates of the beams tested in the Experimental Program described in Chapter 2 is 0.955 Nmm/mm^2, which is the sum of G_F^I being 0.011 Nmm/mm^2, and G_F^{II}, 0.944 Nmm/mm^2. In this example, the 98.9 per cent of the total fracture energy is produced by the descending branch of the bond-slip relationship. Analyzing the different tests compiled on the experimental database, the fracture energy of the bond-slip descending branch, G_F^{II}, represents an average of 98.1 per cent of the total fracture energy, G_F. In terms of energy, this value confirms the importance of performing a non-linear analysis taking into account the descending branch of the bond-slip curve.

3.2.3. Volkersen equation for a single shear loaded joint

Particularizing the Volkersen equation (3.11) for a bilinear bond-slip relationship (as given by equation (3.12)), we can distinguish different stages depending on the force applied at the plate end. The bilinear bond-slip relationship may be divided into three areas depending on the value of the relative displacement between the support and the reinforcement: Zone I (upward branch), Zone II (downward branch), Zone III (horizontal branch) (see Figure 3.10).

By incorporating equation (3.12) into equation (3.11), the governing equation can be solved for both Zones I and II. To facilitate the application of the boundary conditions, the resulting equation is expressed in terms of laminate tensile stress (by using equation (3.9)).

The resulting differential equation related to the upward branch of the bond-slip relationship (Zone I) is given as (3.14).

$$\frac{d^2\sigma_L^I}{dx^2}(x) - \Omega_1^2 \sigma_L^I(x) = 0 \tag{3.14}$$

where:

$$\Omega_1^2 = \frac{1}{E_L t_L}\frac{\tau_{LM}}{s_{LM}} = \frac{1}{E_L t_L}\frac{2G_F{}^I}{s_{LM}^2} = \frac{1}{E_L t_L}\frac{\tau_{LM}^2}{2G_F{}^I} \tag{3.15}$$

Note that for Zone I, the equations are obviously the same as those presented for the elastic range in Chapter 2, provided that:

$$\frac{G_a}{t_a} \approx \frac{\tau_{LM}}{s_{LM}} \tag{3.16}$$

Once in the downward branch of the bond-slip relationship (Zone II), the general expression for the tensile stresses in the laminate can be obtained solving the homogeneous differential equation (3.17).

$$\frac{d^2\sigma_L^{II}}{dx^2}(x) + \Omega_2^2 \sigma_L^{II}(x) = 0 \tag{3.17}$$

where:

$$\Omega_2^2 = \frac{1}{E_L t_L}\frac{\tau_{LM}}{s_{L0} - s_{LM}} = \frac{1}{E_L t_L}\frac{2G_F{}^{II}}{(s_{L0} - s_{LM})^2} = \frac{1}{E_L t_L}\frac{\tau_{LM}^2}{2G_F{}^{II}} \tag{3.18}$$

As mentioned before, in general, the slip value associated to the maximum shear stress s_{LM} is always much lower than the maximum slip value s_{L0}, therefore, in comparing equation (3.15) and (3.18), it can be seen that Ω_2 is much lower than Ω_1. The quotient between Ω_2 and Ω_1, written as equation (3.19), tends to a zero value.

$$\frac{\Omega_2}{\Omega_1} = \sqrt{\frac{s_{LM}}{(s_{L0} - s_{LM})}} = \sqrt{\frac{G_F^I}{G_F^{II}}} \tag{3.19}$$

By solving equations (3.14) and (3.17) with the appropriate boundary conditions, the laminate tensile stress can be obtained. By differentiating its expression and multiplying it by the thickness of the external reinforcement, the shear stress distribution acting on the interface is easily derived, as shown in equation (3.9). Finally, the slip between the support and the external reinforcement is given by the bilinear bond-slip relationship as a function of the shear stresses, as shown in equation (3.12).

3.3. Behavior of a bonded joint prior to the initiation of the debonding process

In the following discussion, the crack propagation process is described through the equations of the stresses that develop during this process. A more detailed description of the deduction of these formulae is shown in Appendix D.

Equations (3.14) and (3.17) can be solved for the particular case of Figure 3.8 either as a function of the applied load at $x = 0$ or alternatively, as a function of a prescribed displacement or a shear stress at the loaded end of the laminate ($s(x = 0)$ or $\tau(x = 0)$). The latter approach is preferred here.

By increasing the value of the prescribed displacement, several load stages can be considered.

3.3.1. Stage 1

Initially (Stage 1, Figure 3.11), the complete interface will be under an elastic state, that is, the interface will be in the upward branch of the relation τ - s (Zone I). Therefore, in Stage 1, cracks will not have appeared in the specimen.

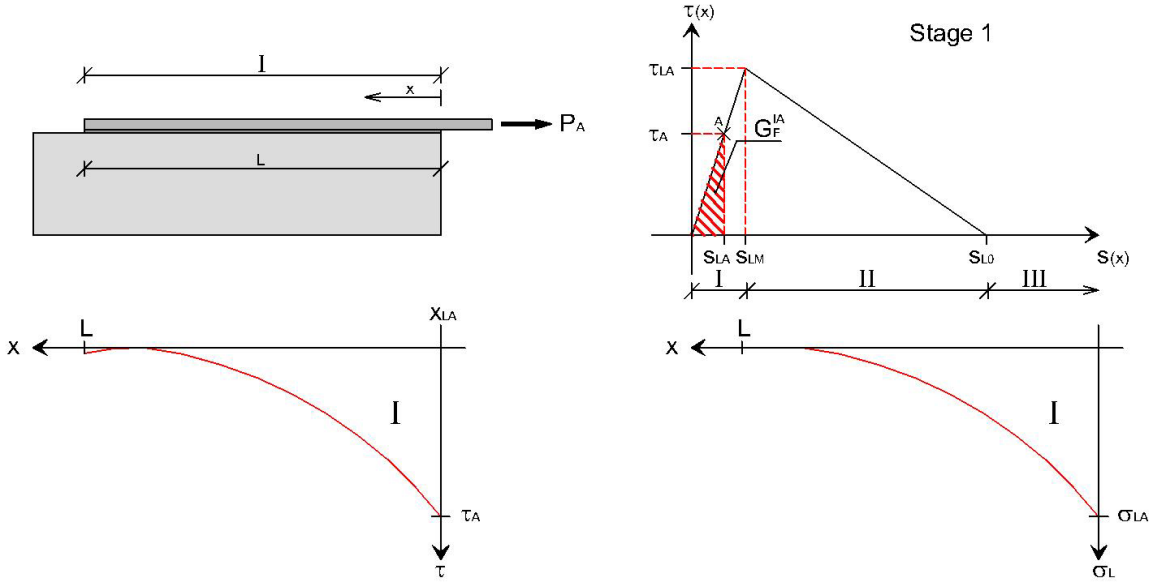

Figure 3.11. Shear and laminate tensile stress distribution in Stage 1.

Equations (3.20) and (3.21) give us the tensile stress distribution in the laminate and the shear stresses on the interface as a function of the shear stress at the loaded end, τ_A.

Zone I: for $0 \le x \le L$

$$\sigma_L^I(x) = -\frac{\tau_A}{t_L \Omega_1} \frac{\sinh(\Omega_1 (L - x))}{\cosh(\Omega_1 L)} \tag{3.20}$$

$$\tau^I(x) = \tau_A \frac{\cosh(\Omega_1(L-x))}{\cosh(\Omega_1 L)} \tag{3.21}$$

Equation (3.21) gives the profile of the shear stress distribution along the laminate. The shear stress diminishes towards the free laminate end. At this location, the shear stress value, given by equation (3.22), approaches zero as the bonded length is long.

$$\tau^I(x = L) = \frac{\tau_A}{\cosh(\Omega_1 L)} \tag{3.22}$$

By particularizing equation (3.20) for $x = 0$, the applied force at the laminate end can be related to the shear stress at the same location. While the shear stress at the loaded end increases to its maximum value, the transferred force increases as well.

$$P_A = \frac{\tau_A}{\Omega_1} b_L \tanh(\Omega_1 L) \tag{3.23}$$

By using equation (3.23), the shear and tensile stresses (equations (3.20) and (3.21) respectively) can be expressed as a function of the applied load at the laminate end.

The applied force can also be expressed as a function of the fracture energy developed up to this moment (equation (3.24)).

$$P_A = b_L \sqrt{2 G_F^{IA} E_L t_L} \tanh(\Omega_1 L) \tag{3.24}$$

These equations are valid as long as τ_A is lower than τ_{LM}. At this moment, the transferred force, which is given by equation (3.25), reaches the maximum value for Stage 1.

$$P_A = \frac{\tau_{LM}}{\Omega_1} b_L \tanh(\Omega_1 L) = b_L \sqrt{2 G_F^I E_L t_L} \tanh(\Omega_1 L) \tag{3.25}$$

3.3.2. Stage 2

When the maximum shear stress τ_{LM} is reached at the loaded end of the laminate, it is said that the interface is under Stage 2. In the bonded connection, two regions can be distinguished. In the first region (Zone I), as the shear stresses increase with the relative displacement, the concrete remains uncracked. In the second region (Zone II) (see Figure 3.12), some microcracks appear in the interface, which is still able to transfer forces. In this case, as long as the load increases, Zone II will increase in length as well, and the maximum shear stress τ_{LM} will move towards the free laminate end. The point where this maximum shear stress is produced is given by the coordinate x_{LM}.

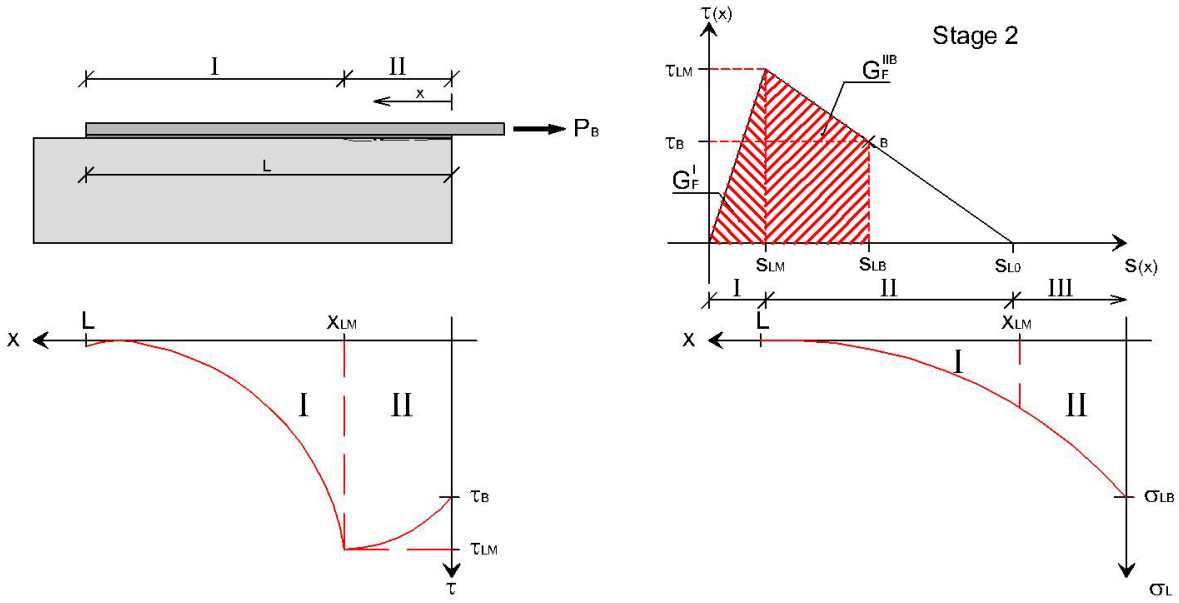

Figure 3.12. Distribution of stresses under Stage 2.

The shear and tensile stress distributions depend on the position of the section under study (Zone I or II) and are given by equations (3.26) to (3.29).

Zone I: for $x_{LM} \le x \le L$

$$\sigma_L^I(x) = -\frac{\tau_{LM}}{t_L \Omega_1} \frac{\sinh(\Omega_1(L-x))}{\cosh(\Omega_1(L-x_{LM}))} \tag{3.26}$$

$$\tau^I(x) = \tau_{LM} \frac{\cosh(\Omega_1(L-x))}{\cosh(\Omega_1(L-x_{LM}))} \tag{3.27}$$

Zone II: for $0 \le x \le x_{LM}$

$$\sigma_L^{II}(x) = \frac{\tau_{LM}}{t_L \Omega_2 \sin(\Omega_2 x_{LM})} \left[\frac{\tau_B}{\tau_{LM}} \cos(\Omega_2(x_{LM}-x)) - \cos(\Omega_2 x) \right] \tag{3.28}$$

$$\tau^{II}(x) = \frac{\tau_{LM}}{\sin(\Omega_2 x_{LM})} \left[\frac{\tau_B}{\tau_{LM}} \sin(\Omega_2(x_{LM}-x)) + \sin(\Omega_2 x) \right] \tag{3.29}$$

where x_{LM} is obtained by solving the following equation:

$$-\frac{\tau_B}{\tau_{LM}} = \frac{\Omega_2}{\Omega_1} \tanh(\Omega_1(L-x_{LM}))\sin(\Omega_2 x_{LM}) - \cos(\Omega_2 x_{LM}) \tag{3.30}$$

The profile of the shear stress distribution given by equations (3.27) and (3.29) is qualitatively shown in Figure 3.12. Along Zone II, the shear stress increases from the load application point to the maximum shear stress location which is the limit between both Zones I and II. As in Stage 1, the shear stress diminishes along Zone I from its maximum value to the free laminate end (equation (3.31)).

$$\tau^{I}(x=L)=\frac{\tau_{LM}}{\cosh(\Omega_1(L-x_{LM}))} \tag{3.31}$$

Note that the shear stress at the free laminate end ($x = L$) approaches zero for long bonded lengths (since x_{LM} has an upper bound as will be shown later on).

Particularizing equation (3.28) for $x = 0$ or integrating the shear stresses along the interface, the force transferred between the concrete and FRP can be obtained as a function of the shear stress τ_B.

$$P_B = b_L \frac{\tau_{LM}}{\Omega_2 \sin(\Omega_2 x_{LM})}\left[1-\frac{\tau_B}{\tau_{LM}}\cos(\Omega_2 x_{LM})\right] \tag{3.32}$$

The applied force can be expressed as a function of the fracture energy that developed up to this moment, as shown in equation (3.33).

$$P_B = b_L\left(\sqrt{2G_F^I E_L t_L}\,\tanh(\Omega_1(L-x_{LM}))\cos(\Omega_2 x_{LM})+\sqrt{2G_F^{IIB} E_L t_L}\,\sin(\Omega_2 x_{LM})\right) \tag{3.33}$$

Stage 2 will be valid as long as the shear stress at the loaded end is higher than the zero value ($\tau_B > 0$) and the length of Zone II, x_{LM}, is lower than the length of the laminate. These limits are analyzed in the next section.

3.3.3. Short and long bonded lengths

During the development of Stage 2, when increasing the slip (or reducing the shear stress) at the loaded laminate end ($x = 0$), the maximum shear stress location given by x_{LM} moves towards the free laminate end. This is obtained by solving equation (3.30). As an example, for a general case of a single shear test with a laminate of 600 *mm* length, Figure 3.13 plots the maximum shear stress location x_{LM} against the decreasing shear stress values at the loaded end.

In a pure shear specimen, two possible situations may arise. In the first one, which will be called a long bonded length, the shear stress at the loaded end reaches a zero value, ($\tau_B = 0$), which is also the end of Stage 2, while x_{LM} is lower than the laminate length. For example in Figure 3.13, at $\tau_B = 0$, x_{LM} is equal to 410 *mm* which is lower than the laminate length of 600 *mm*. Opposite to this situation is the short bonded length, where the length of Zone II, x_{LM}, almost reaches the free laminate end, while the shear stress at the loaded end (τ_B) is greater than zero (so the slip at B is lower than the maximum value s_{L0}). Both situations are better shown in Figure 3.14: a) shows a typical situation for a long bonded length and b) for a short bonded length. For a long bonded length, at the end of Stage 2, the laminate length is long enough to develop the complete profile of shear stresses with both Zones I and II. On the contrary, for a short bonded length, Zone I has almost disappeared before the shear stresses in Zone II have been fully developed.

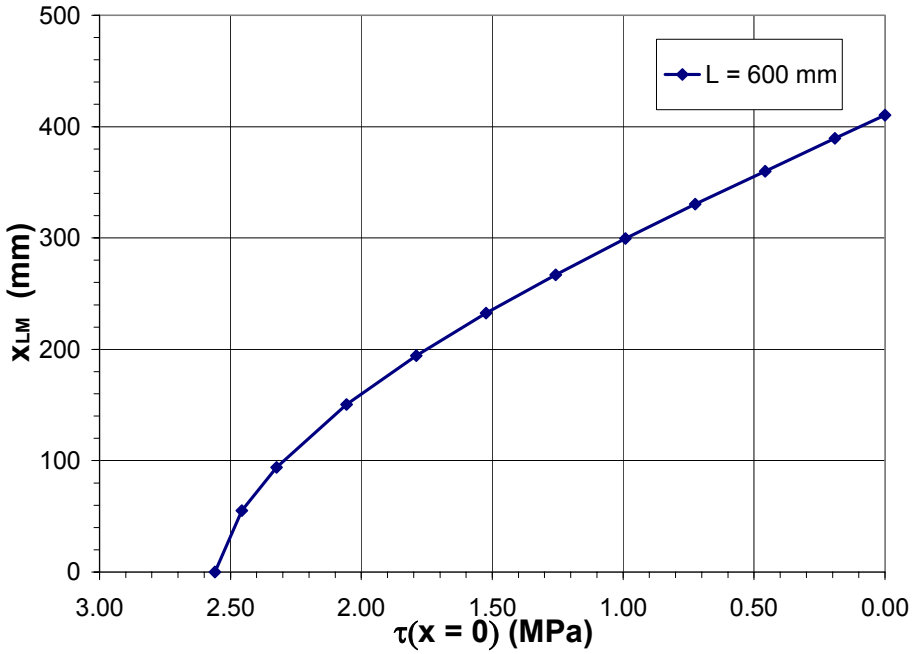

Figure 3.13. Maximum shear stress location along Stage 2 as a function of the shear stress at the loaded end.

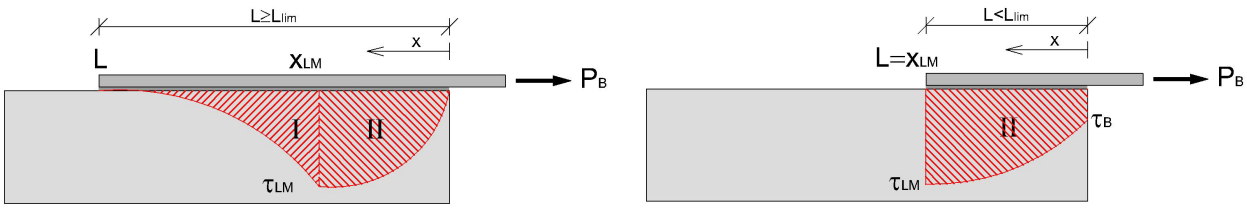

a) Long bonded length b) Short bonded length

Figure 3.14. Long and short bonded length.

In the limit between short and long bonded lengths, the maximum shear stress reaches the free laminate end ($x_{LM} = L$), while the shear stress at the loaded end has already decreased to a zero value ($\tau_B = 0$). By introducing both conditions into equation (3.30), the laminate length that gives the transition between a short and long bonded length is expressed by (3.34).

$$0 = \cos(\Omega_2 L_{\lim}) \quad \longrightarrow \quad L_{\lim} = \frac{\pi}{2\Omega_2} \tag{3.34}$$

From now on, the long bonded length (or long laminate) denomination will comprise those laminates whose lengths are longer than the limit $L_{\lim}$. On the contrary, short bonded lengths (or short laminates) are laminates whose bonded lengths are lower than the limit $L_{\lim}$.

$$L \le \frac{\pi}{2\Omega_2} \qquad \text{Short bonded length (or short laminate)} \tag{3.35}$$

$$L \geq \frac{\pi}{2\Omega_2} \qquad \text{Long bonded length (or long laminate)} \tag{3.36}$$

For the specific case of a laminate whose length is exactly the limit between a short and long bonded length, the transferred force is simplified as equation (3.37).

$$P_B = b_L \frac{\tau_{LM}}{\Omega_2} \tag{3.37}$$

3.3.4. Stage 2 for long bonded lengths

This section presents some observations for pure shear specimens with long bonded lengths during the progress of Stage 2:

Length of Zone II

1) The end of Stage 2 is attained when the shear stress at the laminate loaded end is zero, $\tau_B = 0$. At this point, the length of Zone II is given by incorporating the zero shear stress condition into equation (3.30), as shown in equation (3.38).

$$\frac{\Omega_2}{\Omega_1}\tanh\left(\Omega_1\left(L - x_{LM}\right)\right)\sin\left(\Omega_2 x_{LM}\right) - \cos\left(\Omega_2 x_{LM}\right) = 0 \tag{3.38}$$

   From this condition, it is possible to establish an upper limit for the length of Zone II, that corresponds to the limit length between short and long laminates.

$$x_{LM}\left(\tau_B = 0\right) \leq \frac{\pi}{2\Omega_2} \leq L \tag{3.39}$$

2) If the quotient between Ω_2 and Ω_1 approaches zero (see equation (3.19)), using equation (3.38), the length of Zone II with $\tau_B = 0$ will tend to this upper limit regardless of the laminate length.

$$x_{LM}\left(\tau_B = 0\right) \longrightarrow \frac{\pi}{2\Omega_2} \tag{3.40}$$

3) As mentioned in the previous section, the length of Zone II increases as Stage 2 evolves, that is, with decreasing values of the shear stress (or increasing values of the slip) at the loaded end (see Figure 3.13). This can be justified because the derivative of equation (3.30) with respect to x_{LM}, written as equation (3.41), is negative for any laminate length.

$$\frac{\partial \tau_B}{\partial x_{LM}} = -\tau_{LM}\Omega_2 \tanh\left(\Omega_1\left(L - x_{L_M}\right)\right)\left[\tanh\left(\Omega_1\left(L - x_{LM}\right)\right)\sin\left(\Omega_2 x_{LM}\right) + \right.$$
$$\left. + \frac{\Omega_2}{\Omega_1}\cos\left(\Omega_2 x_{LM}\right)\right] \leq 0 \tag{3.41}$$

4) Since the length of Zone II x_{LM} is a growing function with decreasing values of τ_B, and it has an upper limit, which is given by equation (3.39), the maximum length of Zone II, $x_{LM,\max}$, will be attained at the end of Stage 2. The maximum value $x_{LM,\max}$ is obtained by solving equation (3.38).

5) From equation (3.38), the maximum length of Zone II should be greater than or equal to equation (3.42), since the hyperbolic tangent of Zone I's length, L - x_{LM}, when multiplied by Ω_1 is always lower than or equal to 1.0.

$$x_{LM,\max} \geq \frac{1}{\Omega_2}\arctan\left(\frac{\Omega_1}{\Omega_2}\right) \tag{3.42}$$

6) In case the laminate length is much longer than the limit between a short and long bonded length ($L >> \pi/2$), the laminate will be known as a "substantially long laminate". Under these circumstances, the length of Zone I will be long enough to approach the hyperbolic tangent of $\Omega_1(L - x_{LM})$ by a value of 1.0, $\tanh(\Omega_1(L - x_{LM})) \approx 1.0$. By incorporating this assumption into equation (3.38) for $\tau_B = 0$, the inequality (3.42) turns into (3.43).

$$x_{LM,\max} = \frac{1}{\Omega_2}\arctan\left(\frac{\Omega_1}{\Omega_2}\right) \tag{3.43}$$

7) A critical issue is to determine the limit length between a long laminate and a substantially long laminate. This limit is the sum of the length of Zone II, given by equation (3.43), plus the length of Zone I. The minimum length of Zone I depends on the value of $\Omega_1(L - x_{LM})$ from which the hyperbolic tangent is considered equal to 1.0. Assuming that $\tanh(\Omega_1(L - x_{LM})) \approx 1.0$ is accomplished when $\Omega_1(L - x_{LM})$ is equal to a value greater than n, the laminate will be substantially long when its length is longer than (3.44).

$$L = \frac{1}{\Omega_2}\arctan\left(\frac{\Omega_1}{\Omega_2}\right) + \frac{n}{\Omega_1} \tag{3.44}$$

8) By assuming a reasonable value of n, such as n = 2, which gives $\tanh(\Omega_1(L - x_{LM})) = 0.96$, equation (3.44) can be approached by equation (3.45). From equation (3.45), it can be inferred that the difference between a substantially long laminate and the limit between a short and long bonded length is $1/\Omega_1$.

$$L = \frac{\pi}{2\Omega_2} + \frac{1}{\Omega_1} \tag{3.45}$$

9) In a general example, with typical values of $\Omega_1 = 0.0325$ and $\Omega_2 = 0.0036$, and assuming $n = 2$, the limit length between a short and long laminate is 441 *mm*, and the limit for a substantially long laminate is 471 *mm*. For the last limit, the component representing the length of Zone II, which is 410 *mm* (equation (3.43)), is longer than the length of Zone I, which is 61 *mm*.
10) The maximum length of Zone II ranges from the value given by equation (3.43), which is associated to a substantially long laminate, to $\pi/2\Omega_2$, which corresponds to the limit between a short and long bonded length. Note that the maximum length of Zone II decreases as the total laminate length increases.

$$\frac{1}{\Omega_2}\arctan\left(\frac{\Omega_1}{\Omega_2}\right) \leq x_{LM,\max} \leq \frac{\pi}{2\Omega_2} \tag{3.46}$$

Transferred force

1) For the particular case of a pure shear specimen with a laminate of 600 *mm* length (which was previously commented in Figure 3.13), Figure 3.15 and Figure 3.16 show, respectively, the general increasing trend of the transferred force P_B (given by equation (3.32)) as τ_B decreases, and as the length of Zone II increases. To clarify this trend, equation (3.45) shows the derivative of P_B with respect to x_{LM}. In addition, both Figure 3.15 and Figure 3.16 show that the maximum transferred force is obtained near the end of Stage 2.

$$\frac{\partial P_B}{\partial x_{LM}} = b_L \tau_{LM} \tanh\left(\Omega_1\left(L - x_{LM}\right)\right)\left[\tanh\left(\Omega_1\left(L - x_{LM}\right)\right)\cos\left(\Omega_2 x_{LM}\right) - \frac{\Omega_2}{\Omega_1}\sin\left(\Omega_2 x_{LM}\right)\right] \tag{3.47}$$

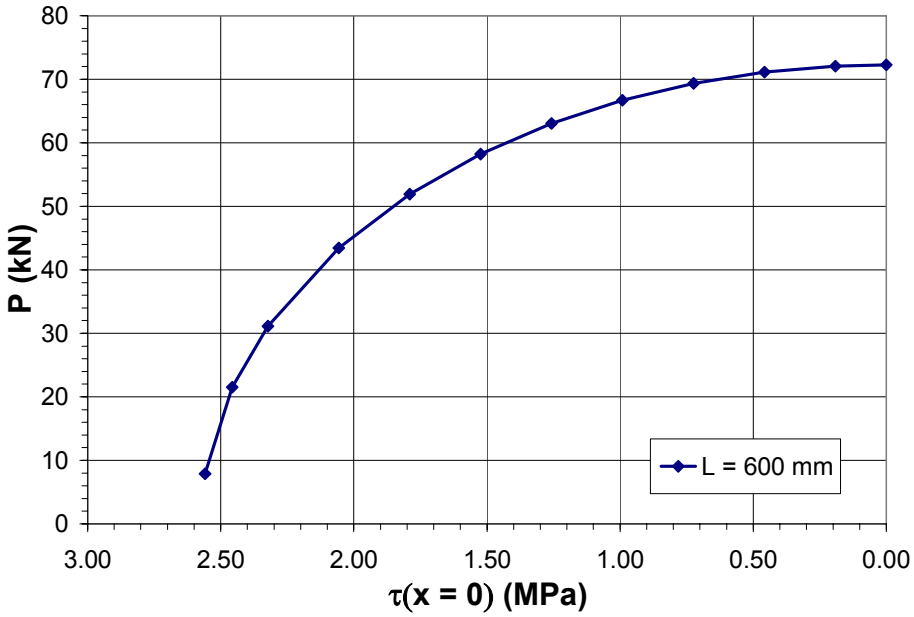

Figure 3.15. Transferred force against the shear stress at the loaded end.

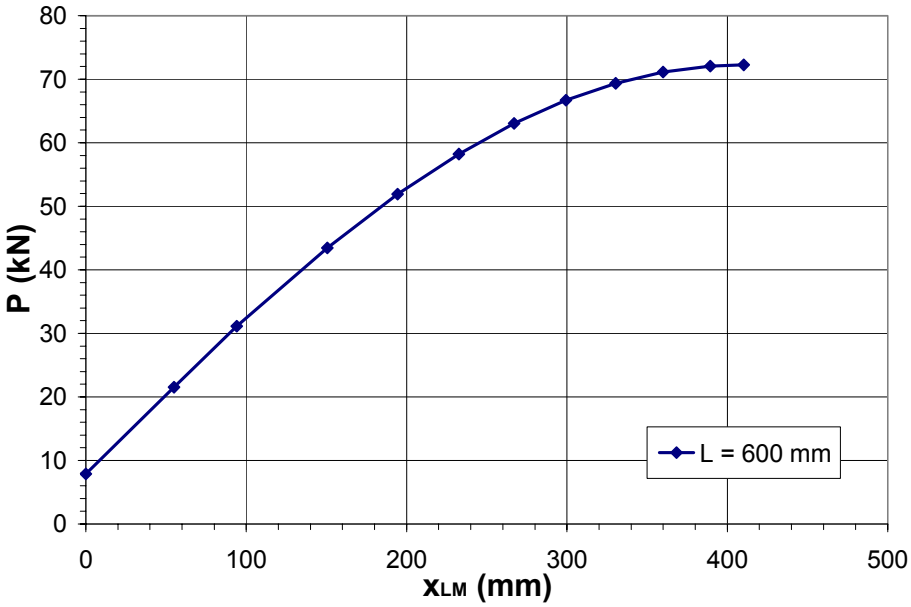

Figure 3.16. Transferred force against the length of Zone II.

2) The maximum transferred force $P_{\max}$ is found by assuming equation (3.47) is equal to zero. If so, equation (3.48) can be obtained. This equation is verified for a particular length of Zone II called $x_{LM,P}$.

$$\tanh\left(\Omega_1\left(L-x_{LM,P}\right)\right)\left[\tanh\left(\Omega_1\left(L-x_{LM,P}\right)\right)\cos\left(\Omega_2 x_{LM,P}\right)-\frac{\Omega_2}{\Omega_1}\sin\left(\Omega_2 x_{LM,P}\right)\right]=0 \quad (3.48)$$

Equation (3.48) is equivalent to accomplishing one of the following conditions:

a) $$\tanh\left(\Omega_1\left(L-x_{LM,P}\right)\right)=0 \quad (3.49)$$

b) $$\tanh\left(\Omega_1\left(L-x_{LM,P}\right)\right)\cos\left(\Omega_2 x_{LM,P}\right)-\frac{\Omega_2}{\Omega_1}\sin\left(\Omega_2 x_{LM,P}\right)=0 \quad (3.50)$$

where $x_{LM,P}$ gives the length of Zone II at the maximum transferred force.

3) Equation (3.49) will only be fulfilled if the maximum shear stress point is located at the end of the laminate, that is $L = x_{LM,P}$. This situation will only be possible in the limit between a short and long bonded length, when the laminate length is equal to $\pi/2\Omega_2$. If so, the transferred force is expressed as (3.51).

$$P_{\max}=b_L\frac{\tau_{LM}}{\Omega_2}=b_L\sqrt{2G_F^{II}E_L t_L} \qquad \left(if \quad L=\frac{\pi}{2\Omega_2}\right) \quad (3.51)$$

4) For a general long bonded length, the value of $x_{LM,P}$ that gives the maximum transferred force ($P_{\max}$) will be the one satisfying equation (3.50). By incorporating $x_{LM,P}$ into equation (3.32), the maximum force that can be applied to a laminate is expressed by equation (3.52).

$$P_{\max} = \frac{b_L \tau_{LM}}{\Omega_2}\left(\frac{\Omega_2^2}{\Omega_1^2}+1\right)\sin\left(\Omega_2 x_{LM,P}\right) \tag{3.52}$$

5) Since the hyperbolic tangent is lower than or equal to 1.0, from the comparison between equation (3.38) and equation (3.50), rewritten as (3.53) and (3.54) respectively, the length of Zone II associated to a maximum transferred force, $x_{LM,P}$, will always be lower than or equal to the maximum length of Zone II, $x_{LM,\max}$.

a) $$\tan\left(\Omega_2 x_{LM,\max}\right) = \frac{\Omega_1}{\Omega_2}\frac{1}{\tanh\left(\Omega_1\left(L - x_{LM,\max}\right)\right)} \tag{3.53}$$

b) $$\tan\left(\Omega_2 x_{LM,P}\right) = \frac{\Omega_1}{\Omega_2}\tanh\left(\Omega_1\left(L - x_{LM,P}\right)\right) \tag{3.54}$$

$$x_{LM,P} \le x_{LM,\max} \le \frac{\pi}{2\Omega_2} \le L \tag{3.55}$$

6) Equation (3.56) shows the shear stress at the loaded end of the laminate ($x = 0$) when the transferred force is at maximum. Since τ_B is not zero, it shows that, in general, the maximum transferred force is not reached at the end of Stage 2. As shown in Figure 3.17, for a 450 *mm* laminate length, the maximum transferred force is achieved when the shear stress at the laminate end is slightly higher than a zero value. However, equation (3.56) clearly shows that the shear stress at the loaded end of the laminate tends to zero as the length of the external reinforcement increases.

$$\tau_B = \tau\left(x=0\right) = \tau_{LM}\cos\left(\Omega_2 x_{LM,P}\right)\left(1-\tanh^2\left(\Omega_1\left(L - x_{LM,P}\right)\right)\right) \tag{3.56}$$

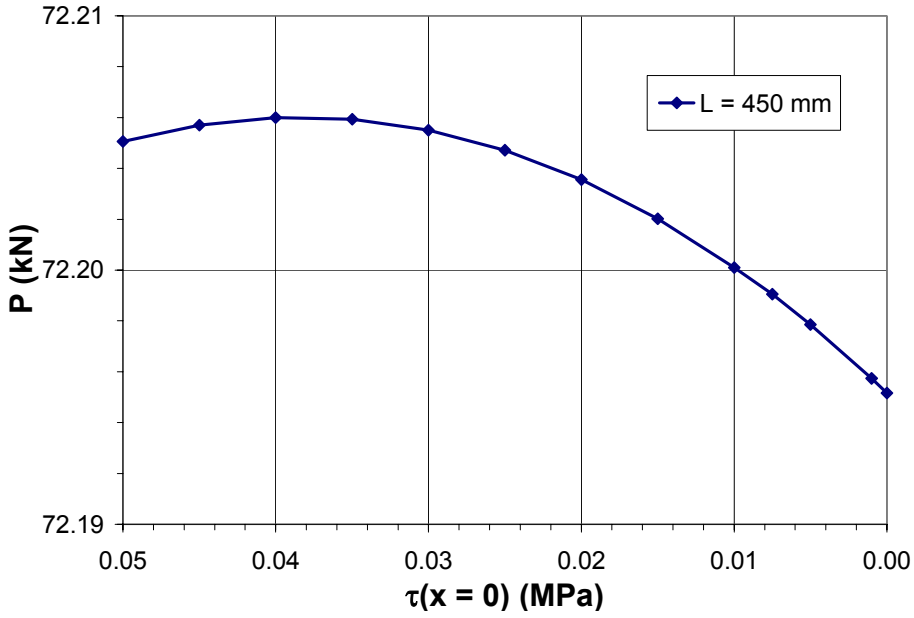

Figure 3.17. Detail of transferred force vs. shear stress at the loaded end for a 450 *mm* laminate.

7) For substantially long laminates ($L >> \pi/2\Omega_2$), both lengths $x_{LM,P}$ and $x_{LM,\max}$ are almost equal since $\tanh(\Omega_1(L - x_{LM})) \approx 1.0$. Thus, in this case, the maximum transferred force is reached when the length of Zone II is almost at maximum, in other words, almost at the end of Stage 2 ($\tau_B = 0$). This is observed in Figure 3.15, where the transferred force for a substantially long laminate of 600 *mm* length is almost at maximum for $\tau_B = 0$. By incorporating the maximum length of Zone II given by equation (3.43) into equation (3.52), the maximum transferred force for a substantially long laminate can be expressed as equation (3.57). As observed, it does not depend on the laminate length.

$$P_{\max} = \frac{b_L \tau_{LM}}{\Omega_2}\left(\frac{\Omega_2^2}{\Omega_1^2} + 1\right)\sin\left(\arctan\left(\frac{\Omega_1}{\Omega_2}\right)\right) \tag{3.57}$$

8) By applying trigonometry and knowing that the total fracture energy G_F is the sum of the fracture energies of Zone I and Zone II (see equation (3.13)), equation (3.57) can be rewritten as shown in (3.58).

$$P_{\max} = b_L\sqrt{2G_F^{\ II}E_L t_L}\left(\frac{G_F^{\ I}}{G_F^{\ II}} + 1\right)\sqrt{\frac{G_F^{\ II}}{G_F^{\ I} + G_F^{\ II}}} = b_L\sqrt{2G_F E_L t_L} \tag{3.58}$$

9) From now on, as a direct consequence of the previous comment, the maximum transference force for a substantially long laminate will be written as equation (3.59). As observed, the maximum transferred force given by (3.59) coincides with the expression derived by using the energy concept of Fracture Mechanics (see equation (3.8)).

$$P_{\max} = b_L\sqrt{2G_F E_L t_L} \tag{3.59}$$

10) As a consequence of the previous comments, a substantially long laminate can also be defined as the laminate length whereby an increase in the bonded length does not imply an increase in the transferred force.
11) The maximum transferred force increases with the laminate length from a value associated to the short/long limit length (given by equation (3.51)) to its maximum value that corresponds to a substantially long laminate given by equation (3.59).

$$b_L\sqrt{2G_F^{II}E_L t_L} \le P_{\max} \le b_L\sqrt{2G_F E_L t_L} \tag{3.60}$$

12) Frequently, the sliding associated to the maximum shear stress (s_{LM}) is very small compared to the maximum sliding (s_{L0}). As a consequence, the fracture energy of Zone II is similar to the total fracture energy ($G_F^{II} \approx G_F$), and the inequality of (3.60) can be approached by equation (3.59).

3.3.5. Stage 2 for short bonded lengths

For short bonded lengths, Stage 2 can be divided into two stages: 2a and 2b, depending on the sliding at the free laminate end.

Stage 2a: $s(x = L) \leq s_{LM}$

Stage 2a has already been described in §3.3.2 as Stage 2. Its formulae are the same for short and long bonded lengths. Stage 2a is initiated when the shear stress reaches its maximum value τ_{LM} at the loaded laminate end ($x = 0$). In addition, it finishes when τ_{LM} reaches the opposite laminate end ($x = L$). Some observations related to this stage, but particularizing for short bonded lengths, are listed below:

1) Similar to long bonded lengths, the length of Zone II, x_{LM}, increases while the shear stress at the loaded end τ_B decreases (or the slip increases).
2) The maximum value of x_{LM} is reached at the end of Stage 2a, when the maximum shear stress reaches the free laminate end. At this point, $x_{LM,\max} = L$.
3) As for long bonded lengths, the transferred force increases as Stage 2a develops.
4) The maximum transferred force will be obtained for a length of Zone II $x_{LM,P}$ that solves equation (3.48), which is valid for both short and long bonded lengths. By solving either condition (3.49) or (3.50), the length of Zone II related to a maximum transferred force is obtained.
5) In particular, equation (3.49) will be fulfilled if the maximum shear stress point is located at the end of the laminate, that is $x_{LM,P} = L$. By incorporating this condition into both equations (3.30) and (3.32), the maximum transferred force is therefore expressed as (3.61). This maximum force will be transferred at the end of Stage 2a, when the maximum shear stress reaches the free laminate end.

$$P_{\max} = b_L \frac{\tau_{LM}}{\Omega_2} \sin(\Omega_2 L) \tag{3.61}$$

6) In this case, the maximum length of Zone II is equal to the length of Zone II that is associated to the maximum transferred force along this stage.
7) For short bonded lengths ($L \leq \pi/2\Omega_2$), equation (3.61) is a growing function of the laminate length since the derivative with respect to L is positive for this range of L values.

$$\frac{\partial P_{\max}}{\partial L} = b_L \tau_{LM} \cos(\Omega_2 L) \geq 0 \tag{3.62}$$

8) In addition, the maximum transferred force is at maximum for L solving equation (3.62) equals to zero. This laminate length is the one associated to the transition between short and long bonded lengths, ($L = \pi/2\Omega_2$). For this laminate length, the transferred force is given by equation (3.63).

$$P_{\max} = b_L \frac{\tau_{LM}}{\Omega_2} \tag{3.63}$$

9) By incorporating $x_{LM,\max} = L$ into equation (3.30), the shear stress at the loaded laminate end is given by equation (3.64). As previously mentioned, in a short

bonded length, this shear stress value at the loaded end corresponds to the end of Stage 2a and the beginning of Stage 2b. At this point, the maximum shear stress reaches the free laminate end. The value of τ_B decreases as long as the laminate length increases. In the limit between a short and long bonded length, τ_B is equal to zero.

$$\tau_B = \tau_{LM} \cos(\Omega_2 L) \tag{3.64}$$

Stage 2b: $s(x = L) > s_{LM}$

Once the maximum shear stress, τ_{LM}, reaches the free laminate end in a short bonded connection, equations developed for Stage 2a are no longer valid. The complete interface is in Zone II of the bond-slip relationship and microcracks may have already appeared along the whole bonded length. From this point on, the interface behavior will be called Stage 2b. Equations (3.65) and (3.66) give the laminate tensile stresses and the shear stresses along the bonded length. Both equations are only valid up to the point when the zero shear stress is reached at the loaded laminate end $\tau_B = 0$.

Zone II: for $0 \le x \le L$

$$\sigma_L^{II}(x) = -\frac{\tau_B}{t_L \Omega_2 \cos(\Omega_2 L)} \sin(\Omega_2 (L - x)) \tag{3.65}$$

$$\tau^{II}(x) = \frac{\tau_B}{\cos(\Omega_2 L)} \cos(\Omega_2 (L - x)) \tag{3.66}$$

Some comments related to Stage 2b are listed below:

1) As shown in Figure 3.18, during Stage 2b, the shear stresses decrease from the free laminate end to the load application point because the complete interface is in Zone II of the bond-slip relationship.

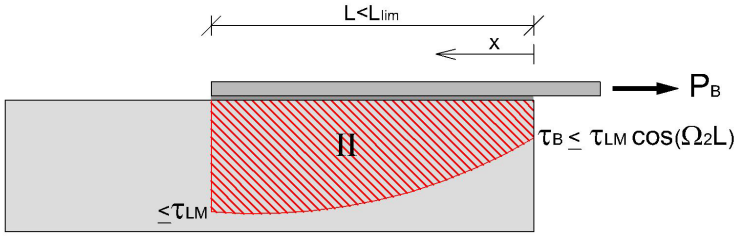

Figure 3.18. Shear stress distribution during Stage 2b.

2) Since the shear stress at the free laminate end during Stage 2b should be lower than or equal to the maximum value, τ_{LM}, the shear stress at the loaded end should accomplish the condition given by equation (3.67).

$$\tau_B \le \tau_{LM} \cos(\Omega_2 L) \tag{3.67}$$

3) Particularizing equation (3.65) for $x = 0$, the force transferred between the concrete and FRP can be obtained as a function of the shear stress at the loaded end.

$$P_B = b_L \frac{\tau_B}{\Omega_2} \tan(\Omega_2 L) \tag{3.68}$$

4) During the evolution of Stage 2b, since the complete bonded length is in Zone II, the shear stresses decrease (or, alternatively, the relative sliding increases) at any location. Since τ_B decreases with the progress of Stage 2b, the transferred force, given by equation (3.68), decreases as well. At the end of Stage 2b ($\tau_B = 0$), the transferred force reaches a zero value. Therefore, the maximum transferred force is developed as Stage 2b starts.

$$P_{B,\max} = b_L \frac{\tau_{LM}}{\Omega_2} \sin(\Omega_2 L) \tag{3.69}$$

5) Accordingly, the evolution of Stage 2b is only possible in circumstances when the slip at the loaded end instead of the applied force is controlled. An attempt to increase the applied force will lead to laminate debonding without the development of Stage 2b.
6) Therefore, when a pure shear test is performed under load control, the laminate debonding is immediately initiated at the end of Stage 2a, since no increase in the transferred force is possible.
7) Figure 3.19 shows the transferred force during both Stages 2a and 2b for a pure shear specimen of 200 *mm* length. As previously mentioned, the maximum force is transferred during the transition between both stages.

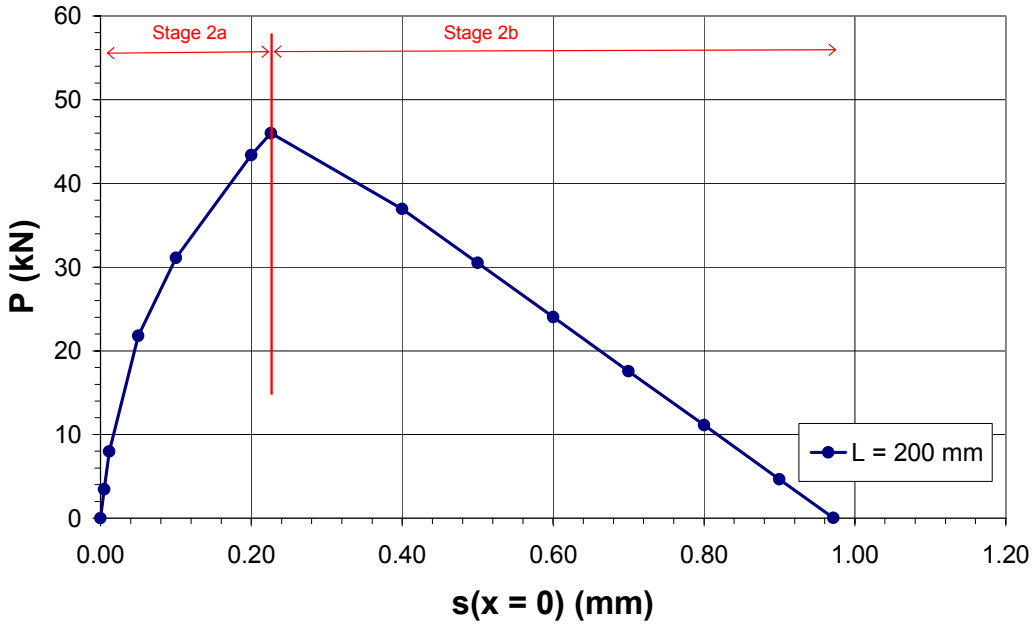

Figure 3.19. Transferred force during Stage 2a and 2b.

8) The maximum transferred force given by equation (3.69) is a growing function of the laminate length, as shown by the derivative of equation (3.69) with respect to the laminate length, which is a positive value (equation (3.70)). The maximum transferred force, given by equation (3.71), corresponds to a laminate length of $\pi/2\Omega_2$, which corresponds to the limit of short and long bonded lengths.

$$\frac{\partial P_B}{\partial L} = b_L \tau_{LM} \cos(\Omega_2 L) \geq 0 \tag{3.70}$$

$$P_{B,\max}\left(L = \frac{\pi}{2\Omega_2}\right) = b_L \frac{\tau_{LM}}{\Omega_2} \tag{3.71}$$

9) This growing trend in the transferred force is shown in Figure 3.20, where the maximum force associated to $\tau_B = \tau_{LM} \cos(\Omega_2 L)$ is plotted for different values of short bonded lengths in a general case of a pure shear specimen.
10) Stage 2b finishes when the maximum sliding s_{L0} is reached at the loaded laminate end and τ_B has decreased to a zero value. From this point on, the stress transfer between laminate and support will no longer be possible ($\tau(x) = 0$). This is shown by incorporating $\tau_B = 0$ into equation (3.65) and (3.66).
11) At the same instant, the maximum sliding is reached not only at the loaded laminate end but also along the complete bonded length. A macrocrack opens, and the laminate suddenly debonds from the concrete surface. At this point, the debonding process of a short bonded length has come to its end.

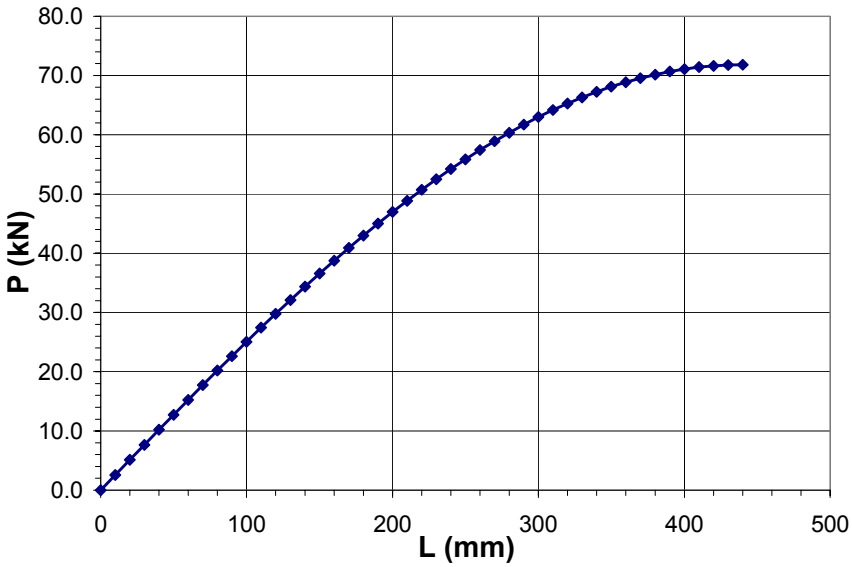

Figure 3.20. Maximum transferred force for short bonded lengths.

3.3.6. Maximum transferred force. Summary

As a summary, the maximum force transferred between the support and the external reinforcement is reached just before the end of Stage 2 for long bonded lengths and at the end of Stage 2a for short bonded lengths. This maximum transferred force can be calculated as:

$$P_{\max} = \begin{cases} \dfrac{b_L \tau_{LM}}{\Omega_2} \sin(\Omega_2 L) & L \le \dfrac{\pi}{2\Omega_2} \\ \dfrac{b_L \tau_{LM}}{\Omega_2} \left(\dfrac{\Omega_2^2}{\Omega_1^2} + 1 \right) \sin(\Omega_2 x_{LM,P}) & L > \dfrac{\pi}{2\Omega_2} \end{cases} \tag{3.72}$$

where:

$x_{LM,P}$: maximum shear stress location solving equation (3.41)

Ω_1 and Ω_2: constants defined by equations (3.15) and (3.18), which are repeated here for the sake of completeness

$$\Omega_1^2 = \frac{1}{E_L t_L} \frac{\tau_{LM}}{s_{LM}} = \frac{1}{E_L t_L} \frac{2G_F^{\ I}}{s_{LM}^2} = \frac{1}{E_L t_L} \frac{\tau_{LM}^2}{2G_F^{\ I}} \tag{3.73}$$

$$\Omega_2^2 = \frac{1}{E_L t_L} \frac{\tau_{LM}}{s_{L0} - s_{LM}} = \frac{1}{E_L t_L} \frac{2G_F^{\ II}}{(s_{L0} - s_{LM})^2} = \frac{1}{E_L t_L} \frac{\tau_{LM}^2}{2G_F^{\ II}} \tag{3.74}$$

As the constants Ω_1 and Ω_2 depend on both the maximum shear stress and the fracture energy of Zones I and II, the maximum transferred force given by equation (3.72) can be alternatively rewritten in terms of fracture energy, as shown in equation (3.75). In addition, substantially long laminates have been distinguished from long laminates in general because of their maximum force which is constant.

$$P_{\max} = b_L \sqrt{2G_F E_L t_L} \begin{cases} \sqrt{\dfrac{G_F^{II}}{G_F}} \sin(\Omega_2 L) & L \le \dfrac{\pi}{2\Omega_2} \\ \sqrt{\dfrac{G_F}{G_F^{II}}} \sin(\Omega_2 x_{LM,P}) & \dfrac{\pi}{2\Omega_2} \le L \le \dfrac{\pi}{2\Omega_2} + \dfrac{1}{\Omega_1} \\ 1 & L > \dfrac{\pi}{2\Omega_2} + \dfrac{1}{\Omega_1} \end{cases} \tag{3.75}$$

It is interesting to note that for short bonded lengths, equation (3.52) gives similar results as equation (3.61), with a small error that increases with the laminate length. As an example, in a typical case of a single shear specimen where different lengths of short laminates have been bonded to the surface, the maximum percentage of error when the transferred force is estimated by using (3.52) is 0.30%. Therefore, equation (3.52) can be used without any distinction regarding the laminate length.

Looking at equations (3.72) and (3.75), it can be observed that the maximum transferred force depends on τ_{LM}, s_{LM}, and s_{L0} or alternatively, τ_{LM}, G_F^I and G_F^{II}. These parameters will be obtained in §3.7.

In the vast majority of cases, the fracture energy of Zone II, G_F^{II}, is almost equal to the total fracture energy, G_F, because the slip associated to the maximum shear stress s_{LM} is very small compared to the maximum value s_{L0}. Therefore, the fracture energy of Zone I is almost zero. As the difference between a long and a substantially long laminate is only an amount of $1/\Omega_1$ that tends towards zero for small values of s_{LM}, equation (3.59) can therefore be used for long bonded lengths (even though they are not substantially long). In conclusion, equation (3.75) can be simplified to equation (3.76) thereby avoiding the resolution of equation (3.48) to find $x_{LM,P}$.

$$P_{\max} = b_L\sqrt{2G_F E_L t_L}\begin{cases}\sin(\Omega_2 L) & L \le \dfrac{\pi}{2\Omega_2} \\ 1 & L > \dfrac{\pi}{2\Omega_2}\end{cases} \tag{3.76}$$

In Figure 3.21, an example of the maximum force related to the laminate length is shown.

For small short bonded lengths, the maximum force can be approximated using Taylor Series as shown in equation (3.77).

$$P_{\max,aprox} = b_L \tau_{LM} L \tag{3.77}$$

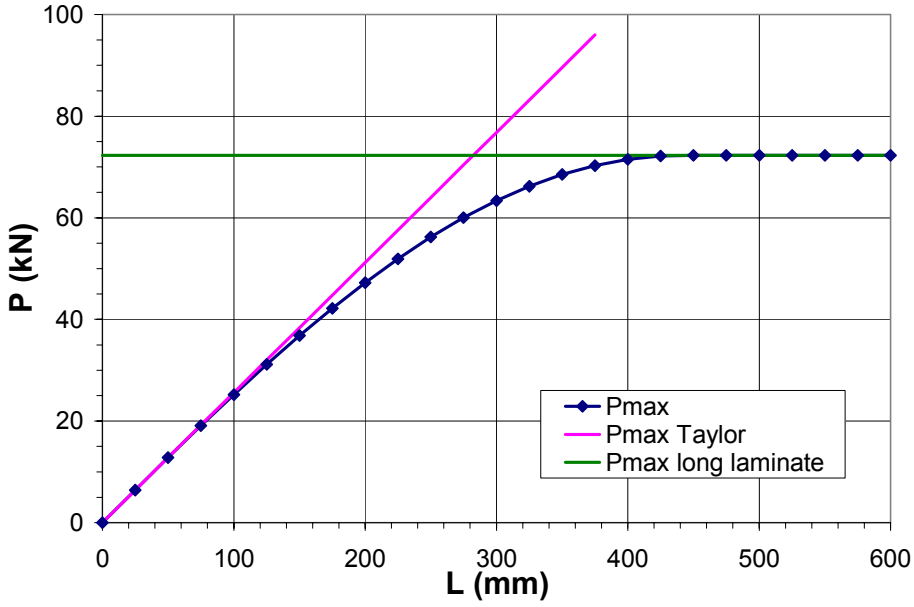

Figure 3.21. Maximum Force P_{max} (*kN*) vs. Bonded Length *L* (*mm*).

At the same time, the theoretical value of the applied load on the laminate establishes an upper limit for the maximum strain on the laminate which depends on the bonded length.

$$\varepsilon_{L,\max} = \sqrt{\frac{2G_F}{E_L t_L}} \begin{cases} \sin(\Omega_2 L) & L \le \dfrac{\pi}{2\Omega_2} \\ 1 & L > \dfrac{\pi}{2\Omega_2} \end{cases} \tag{3.78}$$

3.4. Debonding process

Once the slip at the loaded end of the laminate ($x = 0$) reaches the maximum sliding s_{L0}, the shear stress at this location becomes zero. At this moment, the microcracks turn into a macrocrack, and the debonding process is initiated.

In the following section, the evolution of the interfacial behavior will be described for long bonded lengths. As explained in §3.3.5, for short bonded lengths, the laminate debonds at the end of Stage 2b.

3.4.1. Long bonded lengths

Stage 3a

Stage 3a is initiated with the opening of an interfacial macrocrack, when the slip at the loaded end of the laminate ($x = 0$) reaches the maximum sliding s_{L0}. The laminate can be divided in three regions related to their state: Zone I, II or III (Figure 3.22). The interfacial behavior of Zones I and II is similar to the previous stages. In Zone III, the shear stress is zero and the tensile stress in the laminate is constant. Therefore, no more force can be transferred from the laminate to the support through the length of the real crack x_{L0}. The stress state on the different areas of the bonded laminate can be described by the following equations (from 3.79 to 3.85).

Zone I: for $x_{LM} \le x \le L$

$$\sigma_L^I(x) = -\frac{\tau_{LM}}{t_L \Omega_1} \frac{\sinh(\Omega_1 (L - x))}{\cosh(\Omega_1 (L - x_{LM}))} \tag{3.79}$$

$$\tau^I(x) = \tau_{LM} \frac{\cosh(\Omega_1 (L - x))}{\cosh(\Omega_1 (L - x_{LM}))} \tag{3.80}$$

Zone II: for $x_{L0} \le x \le x_{LM}$

$$\sigma_L^{II}(x) = -\frac{\tau_{LM}}{t_L \Omega_2} \frac{\cos(\Omega_2 (x - x_{L0}))}{\sin(\Omega_2 (x_{LM} - x_{L0}))} \tag{3.81}$$

$$\tau^{II}(x) = \frac{\tau_{LM}}{t_L \Omega_2} \frac{\sin(\Omega_2 (x - x_{L0}))}{\sin(\Omega_2 (x_{LM} - x_{L0}))} \tag{3.82}$$

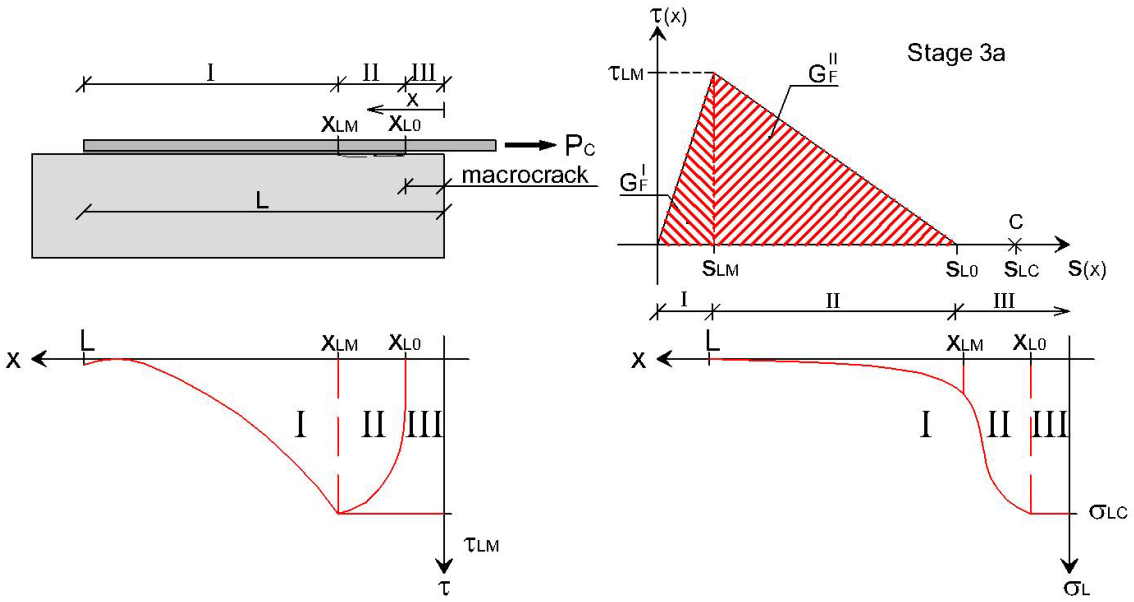

Figure 3.22. Distribution of stresses in Stage 3a.

Zone III: for $0 \le x \le x_{L0}$

$$\sigma_L^{III}(x) = -\frac{\tau_{LM}}{t_L \Omega_2} \frac{1}{\sin(\Omega_2 (x_{LM} - x_{L0}))} \tag{3.83}$$

$$\tau^{III}(x) = 0 \tag{3.84}$$

where the length of Zone II, x_{LM} - x_{L0}, is obtained by solving equation (3.85):

$$\cos(\Omega_2 (x_{LM} - x_{L0}))\left[-\cos(\Omega_2 (x_{LM} - x_{L0})) + \frac{\Omega_2}{\Omega_1}\sin(\Omega_2 (x_{LM} - x_{L0}))\right.$$
$$\left.\tanh(\Omega_1 (L - x_{LM}))\right] = 0 \tag{3.85}$$

This equation is verified if one of the following conditions is accomplished:

a) $$\cos(\Omega_2 (x_{LM} - x_{L0})) = 0 \tag{3.86}$$

b) $$\frac{\Omega_2}{\Omega_1}\sin(\Omega_2 (x_{LM} - x_{L0}))\tanh(\Omega_1 (L - x_{LM})) - \cos(\Omega_2 (x_{LM} - x_{L0})) = 0 \tag{3.87}$$

Equation (3.86) is fulfilled if (x_{LM} - x_{L0}) = $\pi/2\Omega_2$. This situation is only possible when the remaining bonded length (L - x_{L0}) is within the limit between short and long bonded lengths, in other words, when the maximum shear stress is reached at the free laminate end.

For a substantially long bonded length (L - x_{L0}), the hyperbolic tangent of $\Omega_1(L$ - $x_{LM})$ can be approximated as 1.0, $\tanh(\Omega_1(L$ - $x_{LM})) \approx 1.0$. Thus, by incorporating this approximation into equation (3.87), the length of Zone II can be calculated by equation (3.88).

$$x_{LM} - x_{L0} = \frac{1}{\Omega_2}\arctan\left(\frac{\Omega_1}{\Omega_2}\right) \tag{3.88}$$

In Stage 3a, the length of Zone II will range between the value given by equation (3.88) and a maximum value of $\pi/2\Omega_2$.

$$\frac{1}{\Omega_2}\arctan\left(\frac{\Omega_1}{\Omega_2}\right) \le x_{LM} - x_{L0} \le \frac{\pi}{2\Omega_2} \tag{3.89}$$

For a substantially long laminate, the length of Zone II increases as the macrocrack grows. This increasing trend is negligible only until the remaining bonded length equals the minimum length of a substantially long laminate, because the hyperbolic tangent of $\Omega_1(L - x_{LM})$ is still approximated by 1.0. Once the remaining bonded length becomes less than a substantially long length, the macrocrack continues to grow, meanwhile the length of Zone II increases from the value given by (3.88) to a value of $\pi/2\Omega_2$, which corresponds to the end of Stage 3a. Note that Stage 3a finishes when the maximum shear stress reaches the free laminate end.

Since the laminate tensile stress is constant along the macrocrack, equation (3.83) multiplied by the laminate area gives the transferred force along the interface in Stage 3a.

$$P_C = b_L \frac{\tau_{LM}}{\Omega_2 \sin\left(\Omega_2\left(x_{LM} - x_{L0}\right)\right)} \tag{3.90}$$

Again in this case, the applied force at the loaded end can be written as a function of fracture energy.

$$P_C = b_L\left(\sqrt{2G_F^I E_L t_L}\,\tanh\left(\Omega_1\left(L - x_{LM}\right)\right)\cos\left(\Omega_2\left(x_{LM} - x_{L0}\right)\right) + \sqrt{2G_F^{II} E_L t_L}\,\sin\left(\Omega_2\left(x_{LM} - x_{L0}\right)\right)\right) \tag{3.91}$$

The transferred force depends on the length of Zone II, which is obtained from equation (3.87). The derivative of equation (3.90) with respect to x_{LM} is given by equation (3.92). Since the length of Zone II for a long bonded length should be lower than the limit between a short and long laminate, $\pi/2\Omega_2$, the derivative equation (3.92) should be negative. Therefore, the transferred force is a decreasing function with an increasing length of Zone II.

$$\frac{\partial P_C}{\partial x_{LM}} = -b_L \frac{\tau_{LM}}{\Omega_2 \sin\left(\Omega_2\left(x_{LM} - x_{L0}\right)\right)\tan\left(\Omega_2\left(x_{LM} - x_{L0}\right)\right)} \tag{3.92}$$

As a consequence, the transferred force along Stage 3a will be lower than or equal to the transferred force at the end of Stage 2 (given by equation (3.52)).

Figure 3.23 shows the evolution of the transferred force as Stage 3a develops. While the macrocrack grows, the remaining bonded length $L - x_{L0}$ decreases. If the laminate is substantially long, and the remaining bonded length continues to be substantially long,

the length of Zone II will be a constant value given by equation (3.88), and the transferred force will almost remain constant (its slightly decreasing shape can be neglected). However, once the remaining bonded length falls below the value given by equation (3.93), or if the bonded length at the beginning of Stage 3a is not substantially long, the length of Zone II will increase, and the transferred force, which has been almost constant, will start to decrease. Note that the maximum force is transferred at the end of Stage 2 and not along Stage 3a.

$$L - x_{L0} = \frac{1}{\Omega_2}\arctan\left(\frac{\Omega_1}{\Omega_2}\right) + \frac{n}{\Omega_1} \tag{3.93}$$

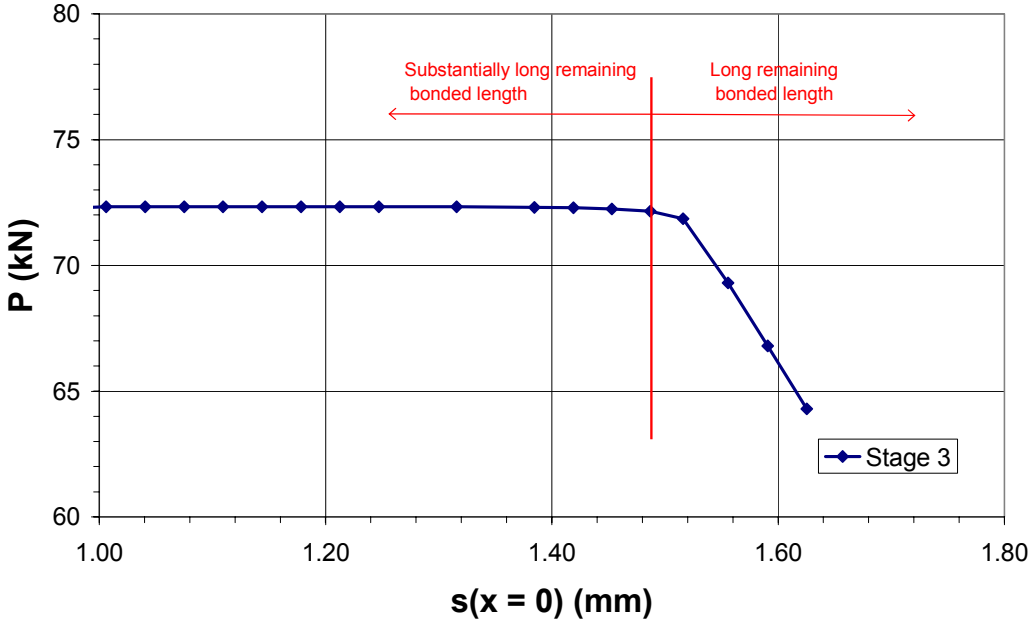

Figure 3.23. Transferred force along Stage 3a.

Finally, when the remaining bonded length is equal to the limit between a short and long laminate (L - $x_{L0} = \pi/2\Omega_2$), that is, when the maximum shear stress reaches the free laminate end, the transferred force can be written as (3.94). From this point on, Stage 3b initiates.

$$P_C = b_L \frac{\tau_{LM}}{\Omega_2} \tag{3.94}$$

In a similar manner as Stage 2b for short bonded lengths, in this case, since the transferred force is a decreasing function with respect to x_{LM}, the evolution of Stage 3a will only be possible when the slip and not the applied force is controlled at the loaded laminate end. If the applied force is attempted to be increased at the end of Stage 2, the debonding of the long laminate will immediately occur and Stage 3a will not happen.

The sliding along the macrocrack length (Zone III) can be calculated as the sum of the maximum sliding acting on the macrocrack tip, s_{L0}, plus the elastic elongation of the laminate (equation (3.95)).

Zone III: for $0 \le x \le x_{L0}$

$$s(x) = s_{L0} + \varepsilon_L(x)(x - x_{L0}) \tag{3.95}$$

Stage 3a is valid until the maximum shear stress is reached at the free laminate end, $\tau(x = L) = \tau_{LM}$. Therefore, Zone I is always present during Stage 3a.

Stage 3b

When the maximum shear stress reaches the free laminate end, Stage 3b will initiate. The complete bonded length will be in Zone II of the bond-slip relationship (see Figure 3.24). Therefore, microcracks will have appeared along the length which still remains bonded. At the beginning of this stage, the remaining bonded length is in the limit between a short and long bonded length. From this point on, the formulae that governs this stage is a function of the tensile force at the loaded laminate end, P_D, as described below:

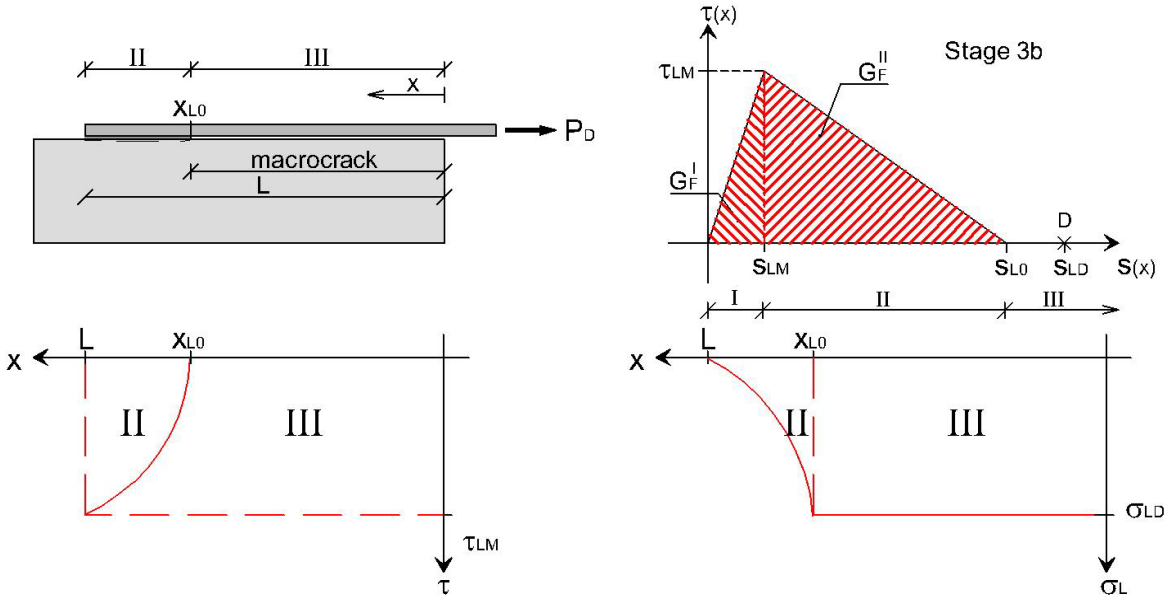

Figure 3.24. Distribution of shear stress at the beginning of Stage 3b.

Zone II: for $x_{L0} \le x \le L$

$$\sigma_L^{II}(x) = -\frac{P_D}{b_L t_L \sin(\Omega_2(L - x_{L0}))}\sin(\Omega_2(L - x)) \tag{3.96}$$

$$\tau^{II}(x) = \frac{P_D}{b_L \sin(\Omega_2(L - x_{L0}))}\Omega_2 \cos(\Omega_2(L - x)) \tag{3.97}$$

Zone III: for $0 \le x \le x_{L0}$

$$\sigma_L^{III}(x) = -\frac{P_D}{b_L t_L} \tag{3.98}$$

$$\tau^{III}(x) = 0 \tag{3.99}$$

At the macrocrack tip, $x = x_{L0}$, the sliding is s_{L0}, so the shear stress is zero. Therefore, equation (3.100) should be accomplished.

$$\tau^{II}(x = x_{L0}) = \frac{P_D}{b_L \tan(\Omega_2 (L - x_{L0}))} \Omega_2 = 0 \tag{3.100}$$

Equation (3.100) is only possible if either (3.101) or (3.102) is verified, in other words, if the applied force at the loaded end P_D is zero or alternatively, if the remaining bonded length is equal to $\pi/2\Omega_2$:

a) $P_D = 0$ (3.101)

b) $\tan(\Omega_2 (L - x_{L0})) = \infty \longrightarrow L - x_{L0} = \pi/2\Omega_2$ (3.102)

Since the shear stress transfer is only possible when the transferred force is different from zero, the macrocrack should not grow anymore as Stage 3b evolves, that is, the remaining bonded length should remain constant and equal to the limit between a short and long bonded length.

For the remaining bonded length (which is in Zone II of the bond-slip curve), the shear stress distribution decreases as Stage 3b develops (Figure 3.25). In addition, the transferred force, which is the sum of shear stresses, diminishes as well. With regard to the slip, it decreases along the macrocrack because the laminate elastic elongation shows the same decreasing trend as that of the transferred force. Along the remaining bonded length, the slip increases up to the maximum sliding value, s_{L0}. The maximum sliding is reached at the same instant at any location of the remaining bonded length. At this point, the macrocrack, which has remained constant along Stage 3b, grows instantaneously from x_{L0} to L. In other words, the laminate completely debonds in a brittle and sudden manner, and the debonding process comes to an end.

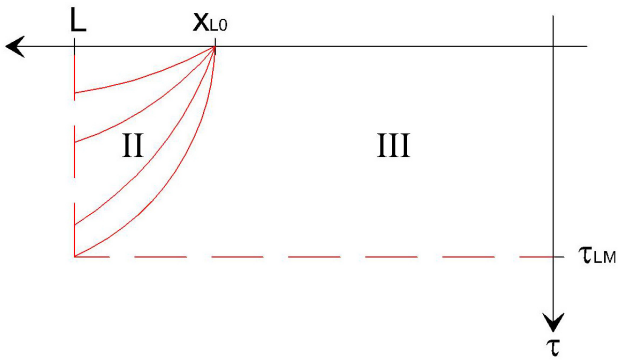

Figure 3.25. Shear stress evolution during Stage 3b.

Stage 3b is only possible when the sliding at the laminate end and not the transferred force is controlled. An increase in the transferred force implies a sudden debonding of the laminate. Note that once the maximum shear stress is reached at the free laminate end in a long bonded length, the sliding at the load application point should decrease to allow the evolution of Stage 3b. This is opposite to the behavior observed in short bonded lengths, where Stage 2b evolves while the sliding at the loaded laminate end increases.

3.4.2. Summary

A brief summary of the sequence of possible stages that can arise during the debonding process is presented in Table 3.1. A distinction between long and short laminates has been made.

Table 3.1. Stages that arise in a pure shear specimen for long and short laminates.

Pure shear specimen				
LONG LAMINATES	Stage 1	Stage 2a	Stage 3a (*)	Stage 3b (*)
SHORT LAMINATES	Stage 1	Stage 2a	Stage 2b (*)	

(*) This stage will arise only if displacement control is performed

3.5. Simplified linear approach

Some authors (Täljsten, 1994; Brosens and Van Gemert, 1998; Neubauer, 2000) gave the maximum load transferred between concrete and laminate by the expression (3.103). For long laminates, equation (3.103) gives the same result as equation (3.59) of §3.3.4 or as the energy approach presented in §3.1.1.

$$P_{\max} = b_L \sqrt{2 G_F E_L t_L} \tag{3.103}$$

The above expression is derived by using the following transformation based on the fracture energy as described by Neubauer (2000). The total fracture energy was previously defined as the area enclosed by the bond-slip relationship. The fracture energy of a bilinear law is the same as the fracture energy of the linear relationship shown in Figure 3.26, with the same maximum shear stress value τ_{LM} and with s_{LM} equal to the maximum sliding s_{L0}. By adopting the linear bond-slip law, and solving the differential equation in Stage 1, the maximum transferred force is given by equation (3.25) by substituting on one hand the fracture energy of Zone I, G_F^I, by the total fracture energy, G_F, and on the other hand s_{LM} by the maximum sliding before debonding occurs, s_{L0}.

$$P_{\max} = b_L \sqrt{2 G_F E_L t_L} \tanh\left(\Omega_1^* L\right) \tag{3.104}$$

where:

$$\Omega_1^{*\,2} = \frac{1}{E_L t_L}\frac{\tau_{LM}}{s_{L0}} \tag{3.105}$$

For long bonded lengths, it is observed that $\tanh(\Omega_1^* L) \approx 1$, and equation (3.105) may be simplified to equation (3.103). However, for short bonded lengths, the value given by (3.103) is only an upper limit and not a good approximation for the maximum applied load.

Finally, the hyperbolic tangent of equation (3.103) can be approached by a parabolic function depending on the limit length between short and long bonded lengths as shown in equation (3.106).

$$P_{\max} = b_L\sqrt{2G_F E_L t_L}\cdot\begin{cases}\dfrac{L}{L_{\lim}}\left(2-\dfrac{L}{L_{\lim}}\right) & L \le L_{\lim}\\ 1 & L > L_{\lim}\end{cases} \tag{3.106}$$

When adopting the linear and fracture energy equivalent bond-slip relationship, the interface shear stress distribution and the laminate tensile stress distribution derived using Stage 1 will not be correct. This approach is only valid for finding the maximum transferred load.

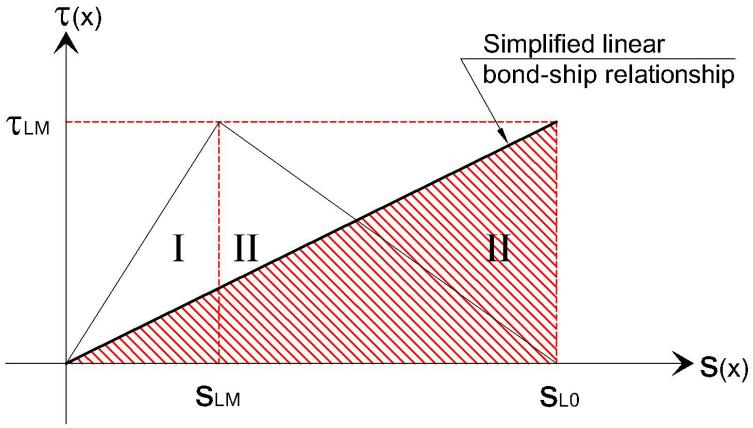

Figure 3.26. Simplified linear bond-slip relationship.

3.6. Existing theoretical models

This section summarizes several of the shear anchorage models that have been developed in the last few years to predict the maximum transferred force between laminate and concrete. These models may be classified into two categories: empirical models based on the regression of test data and models based on Fracture Mechanics theory. Table 3.2 summarizes the maximum transferred force for the various existing models. Note that the same notation was used for all of them to make the comparison easier, even though the notations may be different from their original references in some cases.

The predicted maximum force of Hiroyuki's (1997), Tanaka's (1996) (referenced by Chen and Teng, 2001) and Maeda's (1997) models come from an empirical relationship based on a set of shear experiments. The remaining models are based on Non-Linear Fracture Mechanics. All of the predicted maximum force are very similar except for Van Gemert's (1980) (referenced by Brosens and Van Gemert, 1997) which approximated the shear stress distribution in the full complete length by a triangular function, where the maximum value is located at the loaded end of the laminate and is equal to the concrete tensile strength. Holzenkämpfer's (1994) (referenced by Neubauer, 2000), Täljsten's (1994), Neubauer's (1997, 2000), and Niedermeier's (2000) (referenced by FIB Task Group 9.3 FRP, 2001) models were derived by using the simplified linear approach as described in §3.5. The maximum transferred force according to them is given either by equation (3.104) (Täljsten, 1994; Neubauer, 2000) or by the simplification of (3.106) (Holzenkämpfer, 1994 (referenced by Neubauer, 2000); Neubauer, 1997; Niedermeier, 2000 (referenced by FIB Task Group 9.3 FRP, 2001)). The difference between them relies on the definition of fracture energy and the constants which come from the regression analysis of experimental data. Yuan and Wu (1999)'s (referenced by Chen and Teng, 2001), Chen and Teng's (2001) and Brosens' (2001) models were derived based on Non-Linear Fracture Mechanics by assuming a bilinear bond-slip relationship. Since their procedures are similar to the model developed in §3.3, their predictions on the maximum transferred force are almost identical.

As shown in Table 3.2, Hiroyuki's, Tanaka's and Van Gemert's formulations imply that any given load can be carried by a sufficiently long bonded length. However, this fact is in contradiction with the observed results, which show that any additional bonded length beyond the effective bonded length cannot increase the anchorage strength.

After applying the predictions of these models to the pure shear experimental database presented in Chapter 2, the following conclusions are drawn.

1) Tanaka's and Hiroyuki's models clearly do not fit with the experimental data statistically. They hugely underestimate the bond strength and lead to a very large scatter. The main reason is their dependence on a complete bonded length without considering the existence of an effective length beyond which any increase in the bond length does not increase the transferred force.
2) The model of Maeda was the most robust of the experimental models due to the consideration of this effective bond length.
3) The simplification of Van Gemert's model overestimates the maximum transferred force. The mean average of the ratio test-to-predicted force is 1.75 with the highest coefficient of variation (64%) of the Fracture Mechanics models.
4) The remaining Fracture Mechanics models performed in a similar manner than the model described in this Chapter 3. The statistical performance of this model will be checked in §3.9.

Table 3.2. Summary of maximum transferred force according to the different existing models.

Theoretical model	G_F (Nmm/mm^2)	K	L_{lim} (mm)	P_{max} (N)	
				$L < L_{lim}$	$L \geq L_{lim}$
EMPIRICAL MODELS					
Tanaka (1996)				$b_L L(6.13 - L)$	
Hiroyuki and Wu (1997)				$b_L L(5.88L^{0.669})$	
Maeda et al. (1997)			$e^{(6.13 - 5.80\ln(ELtL))}$	$b_L L_{lim}(110.2 \cdot 10^{-6} E_L t_L)$	-
FRACTURE MECHANICS BASED MODELS					
Van Gemert (1980)				$0.5\ b_L L f_{ctm}$	
Linear elastic approach					
Täljsten (1994)	≤ 1.21	1.0	$2(2G_F E_L t_L)^{0.5}/\tau_{LM}$	$Kb_L(2G_F E_L t_L)^{0.5}\tanh(\tau_{LM}^2 L/2/G_F/E_L/t_L)$	$Kb_L(2G_F E_L t_L)^{0.5}$
Neubauer (2000)	$c_F k_b^2 f_{ctm}$				
Holzenkämpfer (1994)		0.78	$(E_L t_L/4/f_{ctm})^{0.5}$	$Kb_L(2G_F E_L t_L)^{0.5} L/L_{lim}(2 - L/L_{lim})$	
Neubauer (1997)		$0.57/c_F$	$(E_L t_L/2/f_{ctm})^{0.5}$		
Niedermeier (2000)	$0.5c_1^2(f_{ck}/f_{ctm})$		$2(E_L t_L/(f_{cm}/f_{ctm})^{0.5})^{0.5}$		
Non-Linear Fracture mechanics					
Yuan and Wu (1997)	-	1.0	$\pi/2/(\tau_{LM}^2/2/G_F/E_L/t_L)^{0.5}$	$Kb_L(2G_F E_L t_L)^{0.5}\sin(\tau_{LM}^2 L/2/G_F/E_L/t_L)$	
Chen and Teng (2001)	-	0.43	$(E_L t_L/(f_{ctm})^{0.5})^{0.5}$	$Kk_b b_L(E_L t_L(f_{cm})^{0.5})^{0.5}\sin(\pi/2/L_{lim})$	$Kk_b b_L(E_L t_L(f_{cm})^{0.5})^{0.5}$
Brosens (2001)	$c_F\ k_c^2 k_b^2 f_{ctm}$	1.0	$\pi/2/(\tau_{LM}^2/2/G_F/E_L/t_L)^{0.5}$	$Kb_L(2G_F E_L t_L)^{0.5}(s_{L0}/(s_{L0} - s_{LM}))^{0.5}\sin(\tau_{LM}/(s_{L0}\text{-}s_{LM})/E_L/t_L(L - x_{pmax}))$	$Kb_L(2G_F E_L t_L)^{0.5}$
Observations	c_F = constant determined by linear regression analysis of the results of shear tests; k_c = 1.0 for lab tests; c_1 = 0.23 $k_b = (1.125(2 - b_L/b)/(1 + b_L/400))^{0.5}$ (Neubauer, 1997, 2000; Brosens, 2001) or $k_b = (1.125(2 - b_L/b)/(1 + b_L/400))^{0.5}$ (Chen and Teng, 2001) $\alpha = 0$ (Holzenkämpfer, 1994; Neubauer, 1997, 2000; Niedermeier, 2000 (referenced by FIB Task Group 9.3 FRP, 2001); Chen and Teng, 2001) or $\alpha = E_L t_L/E_c/h$ (Täljsten, 1994; Yuan and Wu, 1997; Brosens, 2001)				

3.7. Model parameters

By assuming a bilinear relationship between shear stress and concrete-FRP slip, the application of the model as set out in §3.3 and §3.4 requires the definition of some parameters. All the stress formulae of §3.3 and §3.4 are a function of the maximum shear stress, τ_{LM}, and the constants Ω_1 and Ω_2. Both constants are a function of the maximum shear stress, τ_{LM}, the sliding associated to the maximum shear stress, s_{LM}, and the maximum sliding, s_{L0}. As shown in equations (3.15) and (3.18), as an alternative to the slip values, the fracture energy of Zones I, G_F^I, and II, G_F^{II}, can be used. All of them are a function of both concrete and adhesive properties.

As the sliding associated to the maximum shear stress s_{LM} is much lower than the maximum sliding s_{L0}, the fracture energy of Zone I, G_F^I, is almost zero. Therefore, the total fracture energy is very similar to the fracture energy of Zone II. In this case, if the maximum transferred force is required but there is no interest in obtaining the interfacial stress distribution, the maximum transferred force can be calculated as shown in equation (3.76) which is a function of only two model parameters (instead of three): the maximum shear stress, τ_{LM}, and the total fracture energy, G_F.

3.7.1. Determination of τ_{LM}

The maximum shear stress in the bond-slip relationship, τ_{LM}, is the maximum stress value that can be transferred in a pure shear case. From the tests results compiled on the single/double shear database, in most cases failure was observed to be due to concrete fracture. This means that from all the material components of the interface the weakest link is the concrete. It seems obvious that the maximum shear stress depends on the properties of concrete.

A concrete failure criterion should be applied to determine the value of τ_{LM}.

Applying the Kupfer and Gerstle's criterion (Kupfer and Gerstle, 1973) in a pure shear load case, the maximum shear stress is given by equation (3.107).

$$\tau_{LM} = f_{ctm} \tag{3.107}$$

However, some authors (Holzenkämpfer, 1994; Brosens, 2001) chose the linear Mohr-Coulomb failure to find more accurate expressions. The Mohr-Coulomb line is tangent to both Mohr's circle for pure tension and for pure compression (see Figure 3.27). The equation of the Mohr-Coulomb line can be written as a function of the concrete's compressive and tensile strengths.

$$\tau = \frac{1}{2}\sqrt{f_{cm} f_{ctm}}\left[1 + \left(\frac{f_{cm}}{f_{ctm}} - 1\right)\frac{\sigma_y}{f_{cm}}\right] \tag{3.108}$$

All Mohr's circles tangent to the Mohr-Coulomb line are critical circles and represent a failure situation. Holzenkämpfer (1994) (referenced by Brosens, 2001) determined the

maximum shear stress by using the Mohr-Coulomb line as given by (3.108) and by assuming that in a pure shear state the normal interfacial stresses are zero, as shown by equation (3.109).

$$\tau_{LM} = \frac{1}{2}\sqrt{f_{cm} f_{ctm}} \tag{3.109}$$

The expression for the maximum shear stress given by the FIB Task Group 9.3 FRP (2001) is very similar to that of Holzenkämpfer. The constant c_1, equal to 0.285, was obtained by calibrating the bond model by using simplified experimental tests. It is the same expression as equation (3.109) affected by a factor of 0.57.

$$\tau_{LM} = c_1\sqrt{f_{cm} f_{ctm}} \tag{3.110}$$

As shown in Figure 3.27, if τ_{LM} is defined as equations (3.108) or (3.109), the concrete stress on the longitudinal direction σ_c will be a fixed value given by the circle tangent to the Mohr-Coulomb line in τ_{LM}. Since the concrete axial stiffness is assumed to be much higher than the plate axial stiffness, the concrete stress on the longitudinal direction is zero, $\sigma_c = 0$. In addition, in a pure shear load case, the center of the circle tangent to the Mohr-Coulomb line should be at ($\sigma = 0$, $\tau = 0$), because the principal stresses are $\sigma_I = \tau$ and $\sigma_{II} = \tau$. In that case, as shown in Figure 3.27, the Mohr-Coulomb tangent circle related to the τ_{LM} value given by equation (3.109) is not a pure shear circle. As a consequence, equation (3.109) is not the maximum shear stress in the above case (see Brosens, 2001).

In a pure shear case, the correct value of the maximum shear stress is slightly lower than the value given by (3.109) and it is given by the radius of the pure shear circle tangent to the Mohr-Coulomb line (Figure 3.27).

$$\tau_{LM} = \left(\frac{1}{f_{ctm}} + \frac{1}{f_{cm}}\right)^{-1} \tag{3.111}$$

When compared to the inverse of the tensile strength, the inverse of the compressive concrete strength can be neglected; so equation (3.111) will be derived into equation (3.107). This is a good simplification especially in practical cases because the tensile concrete strength can be easily measured on site by pull-off tests which is a less destructive method than drilling concrete cores to find the concrete compressive strength.

Some authors (Neubauer, 2000; Brosens, 2001) modify the maximum shear stress given by equation (3.111) by multiplying it by two factors: k_c which is the concrete surface influence factor and k_b which represents the width influence. Factor k_c, given by Table 3.3, depends on the surface preparation degree. Factor k_b, given by equation (3.113), represents a combination of the size-effect law of brittle materials and the spreading out of forces in concrete. For a detailed description of both coefficients see Brosens (2001).

$$\tau_{LM} = k_b k_c \left(\frac{1}{f_{ctm}} + \frac{1}{f_{cm}} \right)^{-1} \tag{3.112}$$

where:

$$k_b = \sqrt{\frac{k_e}{1 + \frac{b_L}{b_{L0}}} \left(2 - \frac{b_L}{b_c} \right)} = \sqrt{\frac{k_e}{1 + \frac{b_L (k-1)}{t_{c,ref}}} \left(2 - \frac{b_L}{b_c} \right)} \tag{3.113}$$

In equation (3.113) k_e is an empirical constant which can be calibrated by using experimental results. The value of k_e, which has the smallest standard deviation when predicting the maximum transferred force between concrete and laminate, is given by Brosens as 1.47. The distance in the concrete defined as $t_{c,ref}$, where stresses are influenced by the external reinforcement, is taken as 2.5 to 3.0 times the maximum aggregate size. After analyzing the experimental database of pure shear tests, the value of k_b is found to be between 0.55 and 1.71 for single or double shear tests. Using the same data, the product $k_b k_c$ will be between 0.36 and 1.71 depending on the working conditions.

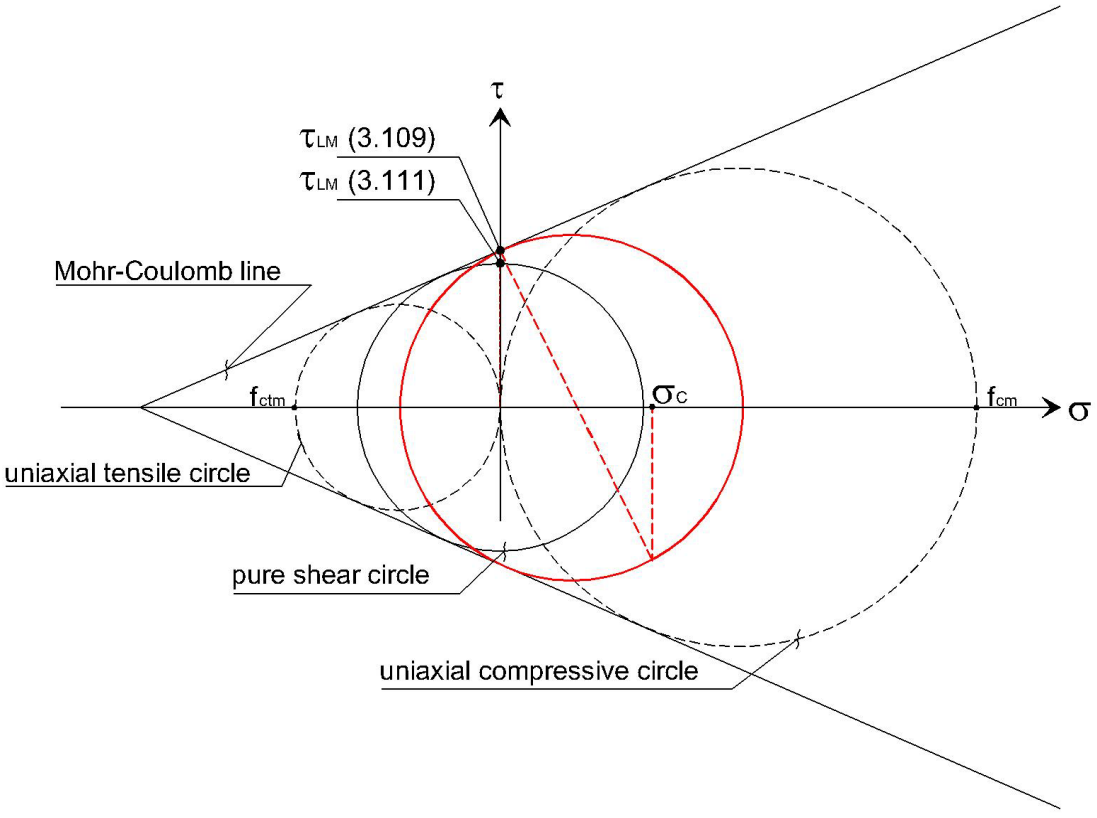

Figure 3.27. Mohr's pure circle.

Table 3.3. Concrete surface influence factor (Brosens, 2001).

k_c	Condition	Example
1.00	Very good	Laboratory environment
0.85-0.95	Good	Indoor applications, good workmanship
0.75-0.85	Normal	Outdoor applications, good workmanship
0.65-0.75	Bad	Dusty and humid environment, poor workmanship

Finally, Neubauer (2000) gives a similar expression for the maximum shear stress based on equation (3.109) but affected by an influenced width factor k_b which is between 1.00 and 1.29 for the shear test database. The constant value of 1.8 comes from the relation between concrete compressive strength and concrete tensile strength.

$$\tau_{LM} = 1.8 k_b f_{ctm} \tag{3.114}$$

where:

$$k_b = 1.06 \sqrt{\frac{1}{1+\frac{b_L}{400}}\left(2-\frac{b_L}{b_c}\right)} \tag{3.115}$$

From all the described formulae, equation (3.112) will be used in the following sections of the present study. This equation comes from the correct interpretation of the Mohr-Coulomb criteria in a pure shear case and was defined by Brosens. Equation (3.112) depends on two factors, the concrete surface influence k_c and the width influence k_b. The factor k_c is given in Table 3.3 and k_b is given by equation (3.113).

3.7.2. Determination of fracture energy G_F

The fracture energy G_F is derived from the area under the curve τ - s. As mentioned in §3.1.1, the fracture energy G_F is defined as the energy by unit area necessary to separate the laminate from the support. Since the concrete forms the weakest link in the bonded connection, the fracture energy should be related to concrete's properties. There are some discrepancies in the definition of this parameter, because in most formulations, this definition comes from an experimental adjustment using single or double shear tests. Barros et al. (2000) summarizes some of the fracture energy expressions given by different authors. The most common formula is that from Holzenkämpfer (1994) (referenced by Chen and Teng, 2001) which has been modified in different occasions afterwards. The fracture energy depends on the concrete tensile strength f_{ctm} and a constant, C_F. The constant C_F is found as the optimal value with the smallest standard deviation when the predicted maximum force is equal to the experimental maximum force applied on the laminate in a single or double shear test. For, C_F the value of 0.092 *mm* was found, but it must be handled with care because it was derived from experiments performed with bonded steel plates (Brosens and Van Gemert, 1998).

$$G_F = C_F f_{ctm} \tag{3.116}$$

Some authors (Holzenkämpfer, 1994; Neubauer, 2000; Brosens, 2001) have introduced the influence of the width k_b and the influence of concrete preparation k_c quadratically in the fracture energy expression (3.116) as shown in equation (3.117). Analyzing the experimental database of pure shear tests, the square of $k_b k_c$ is found to be between 0.13 and 2.94.

$$G_F = k_b^2 k_c^2 C_F f_{ctm} \tag{3.117}$$

Some other authors (Chen and Teng, 2001) have applied both factors k_b and k_c directly to the maximum transferred force expression rather than to the fracture energy expression.

According to Brosens (2001), the value of C_F with a smallest standard deviation for bonded CFRP laminates is between 0.25 *mm* and 0.50 *mm* but the value with the minimum standard deviation is 0.40 *mm*. Neubauer and Róstasy (1997), after analyzing 51 specimens tested in pure shear reported that the value of C_F varied from 0.10 *mm* to 0.30 *mm*, with a mean value of 0.204 *mm* having a standard deviation of 0.053. When making the theoretical maximum transferred force obtained from equation (3.76) equal to the experimental ultimate force in all shear tests of the database described in §2.2.5, C_F shows a mean value of 0.33 *mm* with a standard deviation of 0.15. By comparing these values to that given by Holzenkämpfer (1994), it is observed that the value of C_F is much lower for bonded steel plates than for CFRP laminates. Due to the disparity of values, a further review of this parameter seems necessary. Therefore single or double shear tests reinforced by different material plates should be performed.

In a similar way, the fracture energy was defined by the FIB Task Group 9.3 FRP (2001) as the area under the curve τ - s. In the following expression the constant c_2 is 0.230.

$$G_F = \frac{1}{2} c_2^2 \sqrt{f_{ctm} f_{cm}} = 0.0264 \sqrt{f_{ctm} f_{cm}} \tag{3.118}$$

From all the formulae detailed in this section, equation (3.117) will be used in this work in order to be coherent with the expression of the maximum shear stress chosen.

Once the total fracture energy is known, the fracture energy associated to both Zone I and Zone II can be calculated. For this purpose, the slip associated to the maximum shear stress should be obtained.

3.7.3. Determination of s_{LM}

The slip value s_{LM} at the maximum shear stress τ_{LM} can be found by using the theory of elastic isotropic materials. It can be assumed that the maximum slip on the elastic state (Zone I) is the sum of the slips of each layer which can be expressed as a relationship between the τ_{LM} stress, the thickness and transverse modulus of the different elements that make up the interface which are: a certain influenced thickness in the concrete ($t_{c,ref}$, G_c), the adhesive (t_a, G_a) and the resin between the n layers of the composite laminate (t_r, G_r), when it is not prefabricated. The problem in this equation is to determine the

exact thickness of the adhesive (t_a) and the resin of the composite laminate (t_r), (Brosens, 2001). Typical values of the adhesive transverse modulus G_a are normally between 468 *MPa* and 3692 *MPa*. In general, the value of the resin transverse modulus, G_r, is very similar to the adhesive transverse modulus, G_a.

$$s_{LM} = \tau_{LM}\left(n\frac{t_r}{G_r} + \frac{t_a}{G_a} + \frac{t_{c,ref}}{G_c} \right) \tag{3.119}$$

A similar formula is given by Neubauer (2000) which neglects the influence of adhesive and resin.

$$s_{LM} = 4.5 k_b f_{ctm} \frac{t_{c,ref}}{E_c} \tag{3.120}$$

In the following sections, the slip associated to the maximum shear stress will be calculated by using (3.119).

3.7.4. Determination of s_{L0}

Finally, the relative displacement associated to a zero shear stress value, s_{L0}, is derived from the area under the curve τ - s as shown in equation (3.121).

$$s_{L0} = \frac{2G_F}{\tau_{LM}} \tag{3.121}$$

By defining the fracture energy as equation (3.117), the maximum slip s_{L0} is given by equation (3.122).

$$s_{L0} = 2k_b k_c C_F \left(1 + \frac{f_{ctm}}{f_{cm}} \right) \tag{3.122}$$

The slip when debonding occurs, s_{L0}, was defined by the FIB Task Group 9.3 FRP (2001) as a constant obtained by calibrating the bond model using experimental bond tests. In the following expression the constant c_1 is 0.285 and c_2 is 0.230.

$$s_{L0} = \frac{c_2^2}{c_1} = 0.186\, mm \tag{3.123}$$

As a simplification, if the slip when debonding occurs is calculated by using the Kupfer and Gerstle criterion for the maximum shear stress and the original formula by Holzenkämpfer for the fracture energy, then the value of s_{L0} becomes a constant as well, shown in equation (3.124).

$$s_{L0} = 2C_F \tag{3.124}$$

3.7.5. Summary

In the following sections, the model parameters applied are those given by equations (3.112), (3.117), (3.119) and (3.122).

By using the shear test database presented in Chapter 2, it is possible to obtain a range of typical values for the parameters mentioned above, which are shown in Table 3.4.

Table 3.4. Typical values of the model parameters.

$\tau_{LM} = \left(\frac{1}{f_{ctm}} + \frac{1}{f_{cm}} \right)^{-1}$ (MPa)	from 1.37 to 4.77 *MPa*
$\tau_{LM} = k_b k_c \left(\frac{1}{f_{ctm}} + \frac{1}{f_{cm}} \right)^{-1}$ (MPa)	from 1.01 to 4.60 *MPa*
s_{LM} (*mm*) (equation (3.119))	from 0.004 to 0.057 *mm*
s_{L0} (*mm*) (equation(3.122))	from 0.241 to 1.746 *mm*
G_F (*MPa·mm*) (equation (3.117))	from 0.132 to 3.368 *MPa·mm*

3.8. Application of the proposed formulae to a single shear test example

To better understand the formulation described in the previous section, two examples of a generic single shear test with CFRP laminates are presented.

The studied examples consist of a concrete specimen with a compressive strength of 35 *MPa* strengthened with a pultruded CFRP laminate of 100 *mm* x 1.40 *mm* with a longitudinal elastic modulus of 150 *GPa*. Assuming a bilinear bond-slip relationship, the model parameters obtained applying the formulae of §3.7 are the following: τ_{LM} = 2.46 *MPa*, s_{LM} = 0.012 *mm*, and s_{L0} = 0.972 *mm*.

By using these values, the limit between short and long bonded lengths is found to be 441 *mm*. The limit between long and substantially long laminates is 471 *mm*. Two different laminate lengths are studied: 200 *mm* which corresponds to a short laminate and 600 *mm* which is a substantially long bonded length.

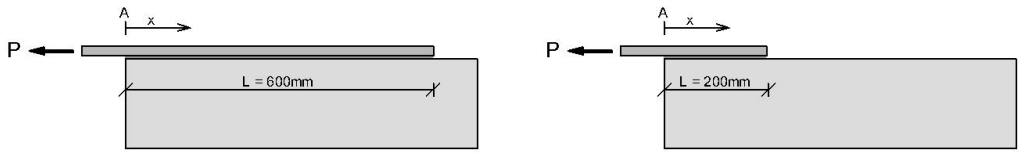

Figure 3.28. Long bonded length of 600 *mm*. Short bonded length of 200 *mm*.

3.8.1. Long bonded length example (*L* = 600 *mm*)

In Figure 3.29, the shear stress distribution during both Stages 1 and 2a is shown along the external reinforcement as a function of the applied load and the relative sliding at the loaded end of the laminate, s(x = 0). For low load levels (during Stage 1) the shear stresses are concentrated near the load application point. Once the maximum shear stress τ_{LM} is reached at this location, under 7.8 *kN*, Stage 2a is initiated. From this moment on, as the load level increases, the maximum shear stresses location x_{LM} moves towards the free laminate end. As observed in Figure 3.29, in this example there is enough bonded length for the complete development of Zone II before the maximum shear stress τ_{LM} reaches the free laminate end.

Figure 3.30 shows the evolution of shear stress along Stage 3a that appears once the relative sliding at the loaded end of the laminate has reached its maximum value s_{L0}. At this point in time, the debonding process is initiated and a real macrocrack starts its propagation so long as the relative displacement between the support and the external reinforcement increases above s_{L0} at the load application point. As shown in the bilinear bond-slip relationship of Figure 3.10, the shear stresses along the macrocrack (Zone III) are zero.

For long bonded lengths, the distance x_{LM} - x_{L0} slightly increases with the macrocrack growing from the beginning of Stage 3a (as observed in Figure 3.31). However once the remaining bonded length decreases to the minimum length for a substantially long laminate, the length of Zone II increases significantly. In this case, the length of Zone II is 410 *mm* at the beginning of Stage 3a. At the end of this stage, this length has increased to 441 *mm*. At this point, the remaining bonded length is equal to the limit between short and long bonded lengths.

Stage 3a finishes when the maximum shear stress reaches the free laminate end. Then, Stage 3b initiates. From this point on, the macrocrack length does not continue growing. The shear stresses start to decrease to a zero value along the remaining bonded length as Stage 3b evolves (Figure 3.32). When the shear stress reaches a zero value at any location, a brittle debonding of the laminate occurs. At this point, the macrocrack length increases from the value at the beginning of Stage 3b, which is the limit between short and long bonded lengths, to the complete laminate length.

As shown in Figure 3.29, during Stage 1 and 2, the shear stresses are almost zero at the free laminate end. However during Stage 3a, the more the macrocrack length x_{L0} increases, the greater the shear stress at the free laminate end. During Stage 3b, the shear stress distribution is at maximum at the free laminate end. At this location, the shear stress decreases to zero with the evolution of Stage 3b.

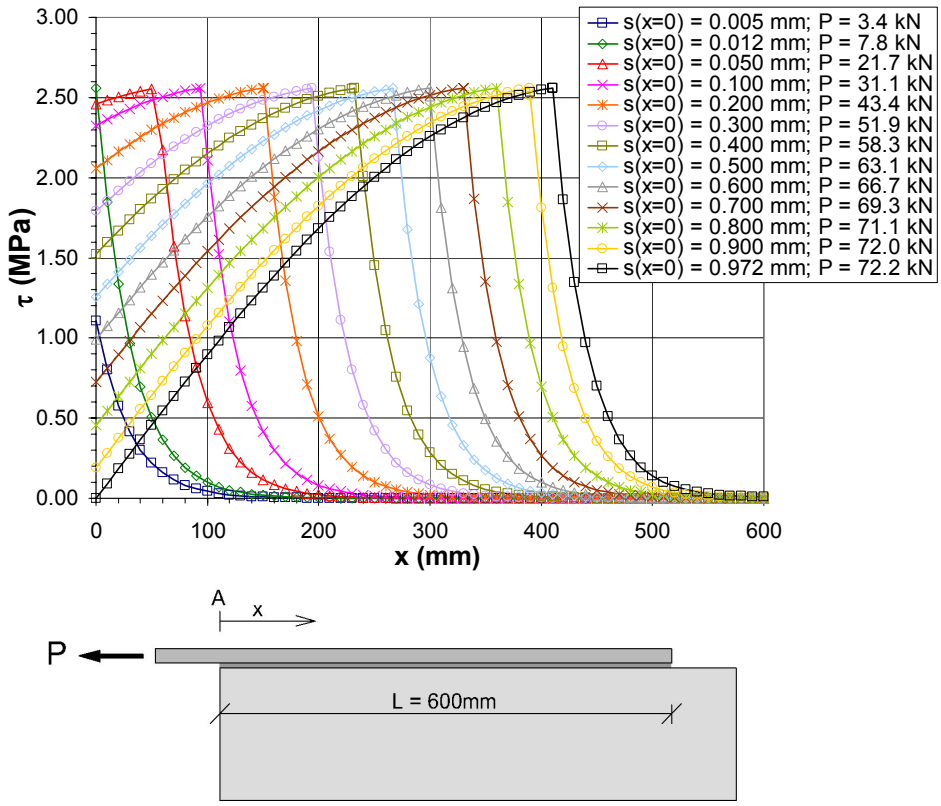

Figure 3.29. Shear stress distribution during Stages 1 and 2 depending on the slip value at $x = 0$.

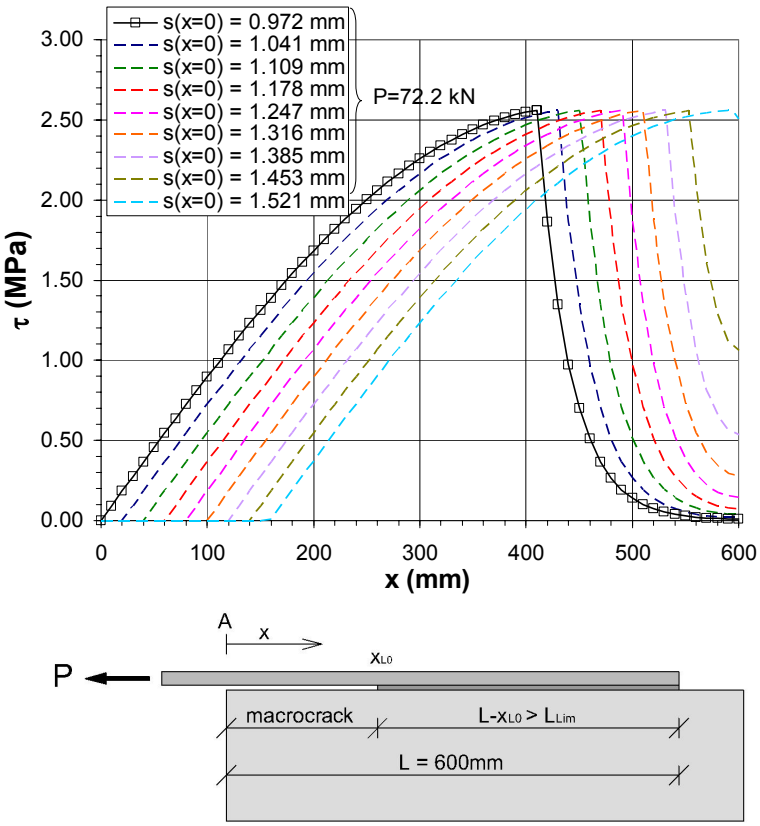

Figure 3.30. Shear stress distribution during Stage 3a depending on the slip value at $x = 0$.

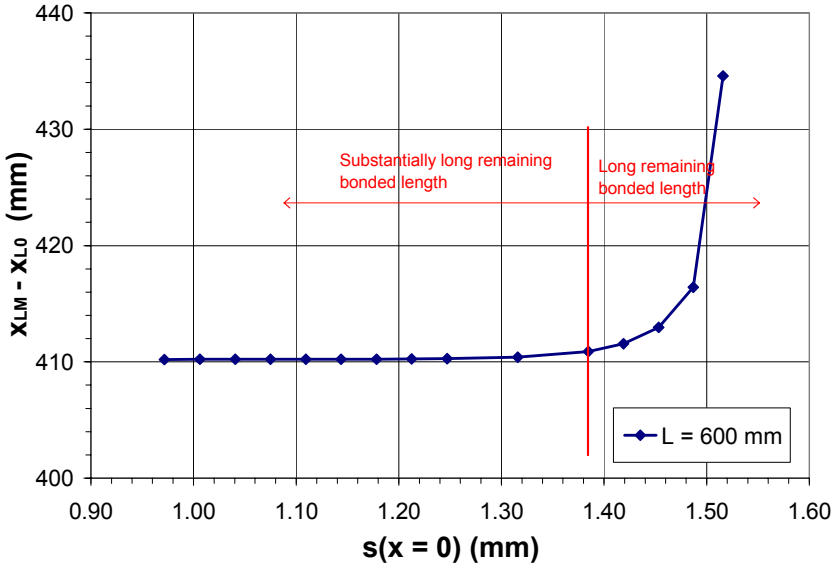

Figure 3.31. Evolution of Zone II's length along Stage 3.

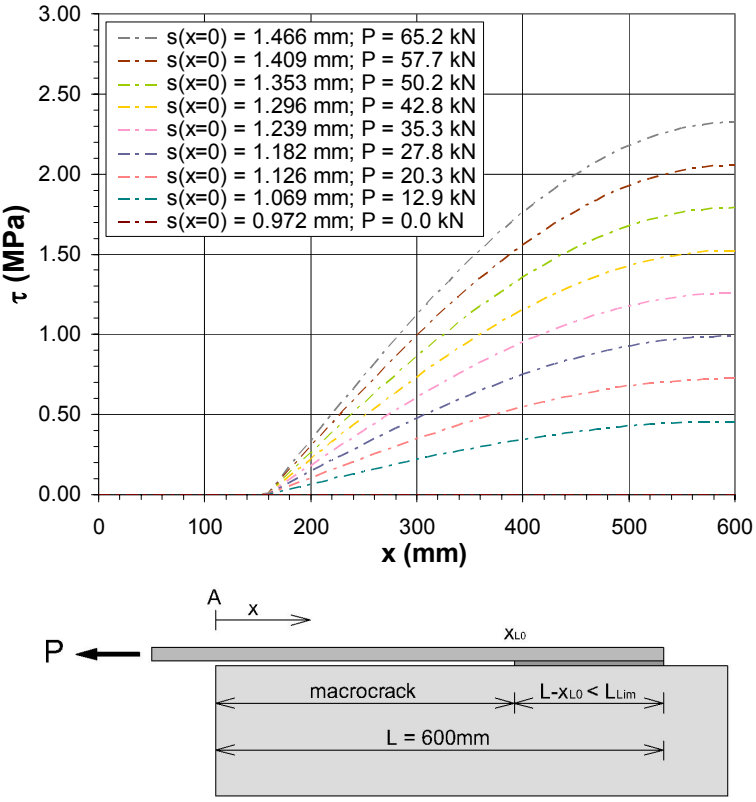

Figure 3.32. Shear stress distribution during Stage 3b depending on the slip value at $x = 0$.

Figure 3.33 shows the tensile stress distribution during Stages 1 and 2. The maximum tensile stress is always located at the loaded end of the laminate. Its maximum value is 516.2 *MPa*. This value is associated to a maximum strain of 3440 $\mu\varepsilon$ (0.34%) which is much lower than the value of 0.6 - 0.8% given by some recommendations (see Chapter 2, §2.2.3) to avoid peeling failure.

The tensile stress in the transition point between Zone I and II, designed as x_{LM}, is almost constant for the different load stages. In this example, this value is 56.3 *MPa* which represents 10.9% of the maximum tensile stress.

$$\sigma_L\left(x = x_{LM}\right) \approx \frac{\tau_{LM}}{t_L \Omega_1} \tag{3.125}$$

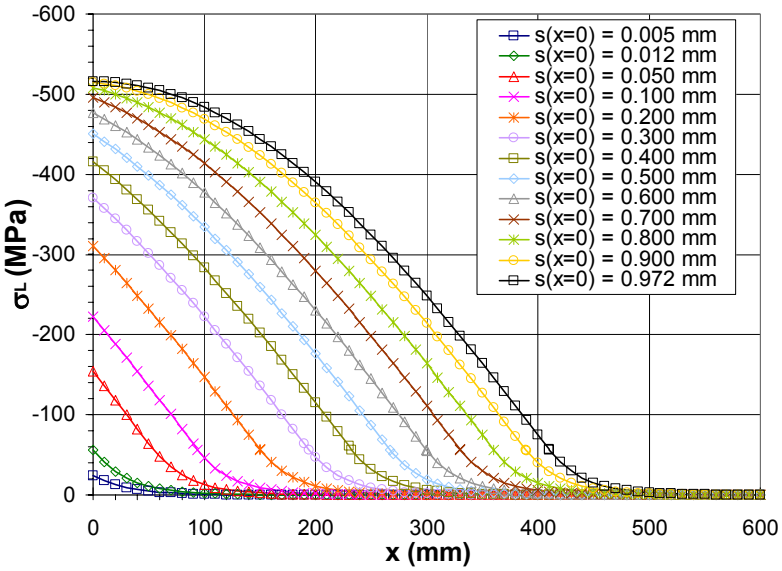

Figure 3.33. Laminate tensile stress distribution during Stages 1 and 2 depending on the slip value at $x = 0$.

In Figure 3.34 the tensile stress distribution during Stage 3a is given. While the relative sliding is increasing at the loaded laminate end, the tensile stress distribution along the debonded length x_{L0} remains constant (the shear stresses are zero). Although it cannot be clearly appreciate in Figure 3.34, the tensile stress at the laminate loaded end slightly decreases with the evolution of Stage 3a.

Figure 3.35 shows the laminate tensile stress distribution along the remaining bonded length during Stage 3b. The laminate tensile stress diminishes at any location as Stage 3b develops. When fixing a plotted line associated to a slip value, the laminate tensile stress is constant along the macrocrack length obtained at the end of Stage 3a, x_{L0}. At the end of Stage 3b, the laminate completely debonds since the laminate tensile stress has decreased to a zero value at any location.

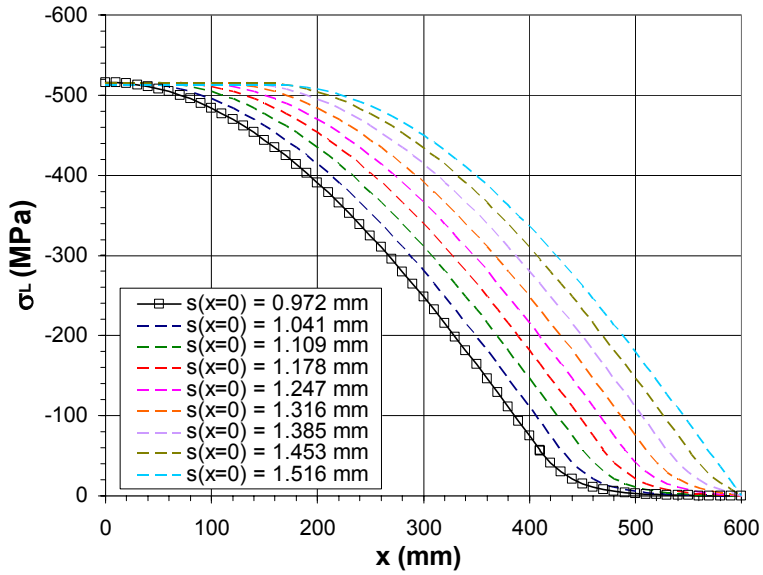

Figure 3.34. Laminate tensile stress distribution during Stage 3a depending on the slip at $x = 0$.

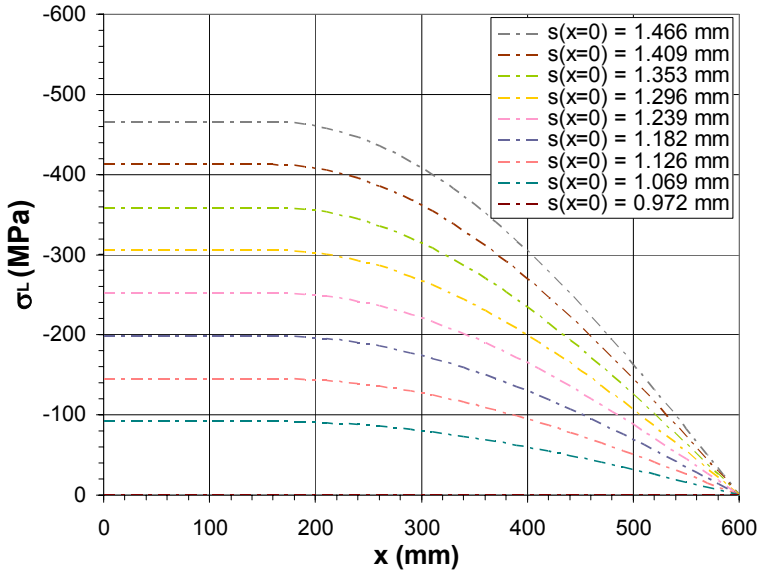

Figure 3.35. Laminate tensile stress distribution during Stage 3b depending on the slip at $x = 0$.

The transferred force between concrete and laminate is obtained in Figure 3.36 for different values of sliding at the loaded end of the laminate. This is done either by evaluating the tensile stress at the loaded laminate end or by finding the integral of the shear stress distribution along the reinforcement. The maximum transferred force (72.2 *kN*) is obtained near the transition between Stage 2 and Stage 3a, just before the sliding at the loaded end of the laminate reaches the maximum relative displacement, s_{L0}. As mentioned before, when s_{L0} is reached at the laminate loaded end, Stage 3a starts and a macrocrack appears. As observed in Figure 3.36, during Stage 3a, at increasing sliding values at the loaded laminate end, the transferred load will remain almost constant until the remaining bonded length falls below the length associated to a substantially long laminate. From this point on, the transferred force slightly decreases until the maximum shear stress reaches the free end of the laminate. Thereafter, a

macrocrack opens in part of the interface and the remaining bonded length displays microcracks. When Stage 3b initiates, the transferred force decreases with decreasing values of the sliding at the laminate loaded end. Therefore, Stage 3b is only possible when the slip is controlled at the loaded end. An increase in the transferred force will lead to the sudden laminate debonding.

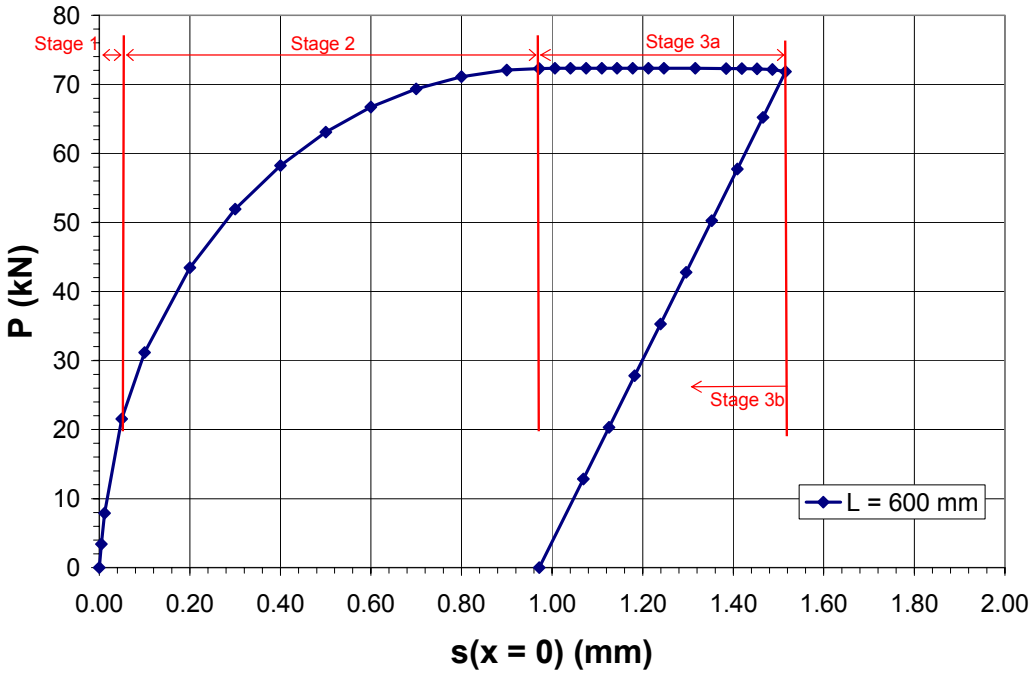

Figure 3.36. Transferred force vs. relative sliding at the loaded end of the laminate.

In Figure 3.37, the relative displacement between the concrete and the laminate during Stages 1 and 2 is shown. A decrease of the sliding from the load application point ($x = 0\ mm$) to the free laminate end ($x = 600\ mm$) is observed. The decreasing slope is more pronounced along Zone II. In general, this can be explained by the fact that the maximum shear stress is associated to a small relative sliding given by s_{LM}. Therefore, between the maximum shear stress location and the free laminate end (Zone I), the relative displacement is almost zero. It should be mentioned that the sliding at the free laminate end is very small but different from zero because it is not restricted.

Stage 3a starts when the loaded laminate end reaches the maximum sliding s_{L0}. At this moment, a macrocrack appears near the load application point. The sliding along the debonded length is calculated as the maximum sliding s_{L0} plus the elastic elongation of the laminate. Figure 3.38 shows the relative displacement between concrete and laminate during Stage 3a. The macrocrack length is clearly defined by those locations where the sliding is higher than the maximum value of Zone II, s_{L0}.

When the maximum shear stress reaches the free laminate end, Stage 3b will initiate. Figure 3.39 shows the relative sliding during Stage 3b. As the transferred force decreases with the development of this stage, so does the elastic elongation of the laminate. Therefore, the relative sliding along the macrocrack, which is the sum of the maximum sliding plus the elastic elongation, will decrease with the evolution of Stage 3b. However, the slip along the bonded length increases up to point where the

maximum sliding is reached at any location. Figure 3.39 shows that the slip at the macrocrack tip, x_{L0}, remains constant regardless of the slip at the loaded laminate end. In addition, it can be observed that once Zone I disappears from the complete interface, the relative displacement at the free laminate end is more significant.

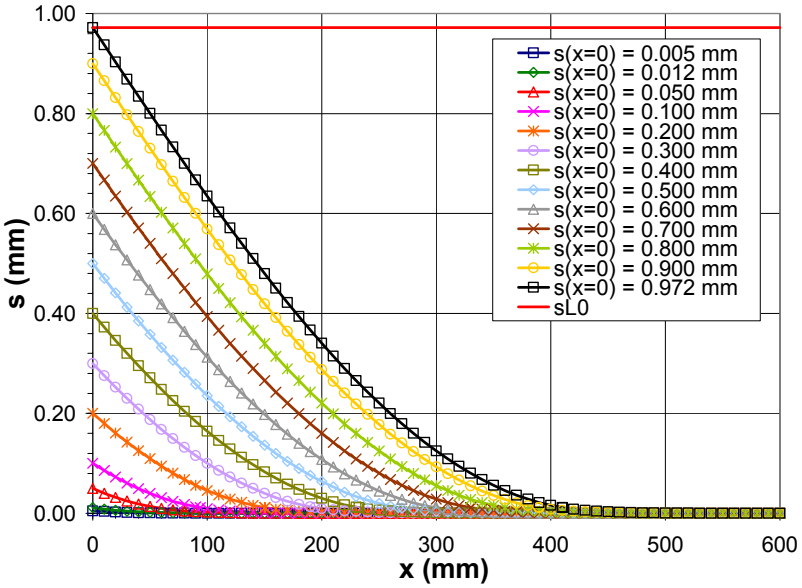

Figure 3.37. Relative sliding during Stages 1 and 2 depending on the slip value at $x = 0$.

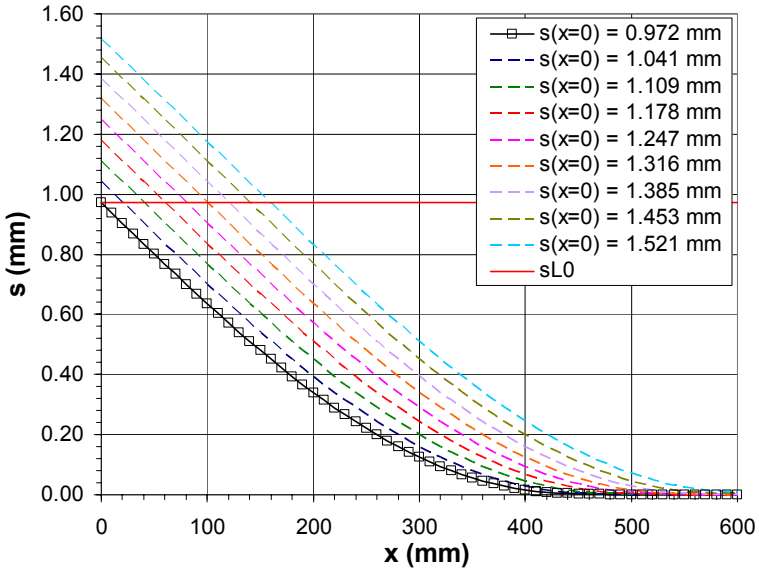

Figure 3.38. Relative sliding during Stage 3a depending on the slip value at $x = 0$.

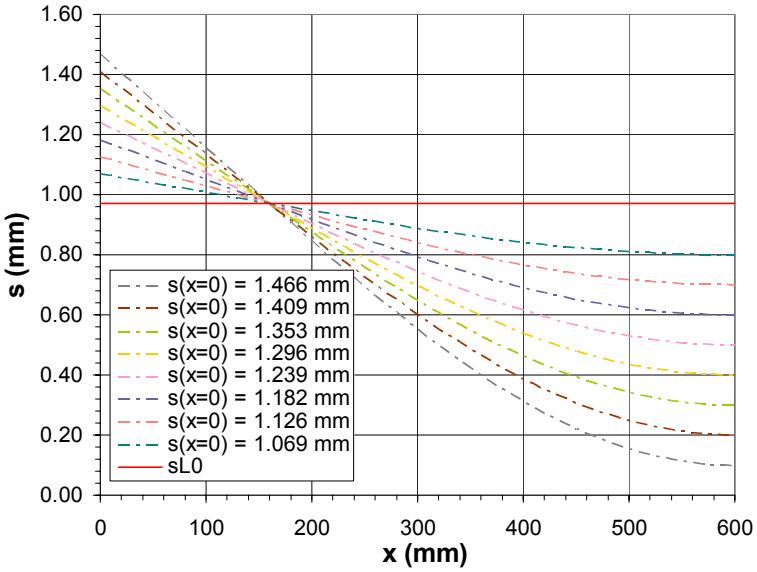

Figure 3.39. Relative sliding during Stage 3b depending on the slip value at $x = 0$.

3.8.2. Short bonded length example (L = 200 *mm*)

In the following, a single shear test with a 200 *mm* bonded laminate is analyzed. The same parameters as the previous example are used in this case.

Figure 3.40 shows the shear stress distribution during Stages 1 and 2a of the debonding process. First, the interface behaves in a linear elastic way up to an applied load of 7.8 *kN*, which corresponds to the end of Stage 1. Then, Stage 2a is initiated with the development of microcracks along part of the bonded connection (Zone II). Looking at the shear stress distribution of Figure 3.40, the main difference with the long bonded length example is that there is not enough length for the complete development of the shear stresses of Zone II.

Once the maximum shear stress τ_{LM} reaches the free laminate end, Stage 2b is initiated. The complete laminate is in Zone II of the bond-slip curve, and microcracks could appear along the complete length of the interface. During Stage 2b, as shown in Figure 3.41, the shear stress profiles decrease with increasing values of the sliding at the loaded laminate end, $s(x = 0)$. Therefore, the maximum stress is always lower than the maximum value τ_{LM}. This phenomenon can be explained by the fact that in the downward branch of the bilinear bond-slip relationship (Zone II), as long as the sliding increases, the shear stresses decrease to a zero value associated to the maximum relative displacement, s_{L0}. In addition, the slope of the plotted lines decrease with the development of Stage 2b (from $s(x = 0) = 0.246$ *mm* until s_{L0}).

As Stage 2b evolves, microcracks rise in length and number until they turn into a macrocrack at the end of Stage 2b. Thereafter, the shear stresses decrease to a zero value at any location. Since the macrocrack extension is equal to the laminate length, the laminate debonds along its full length.

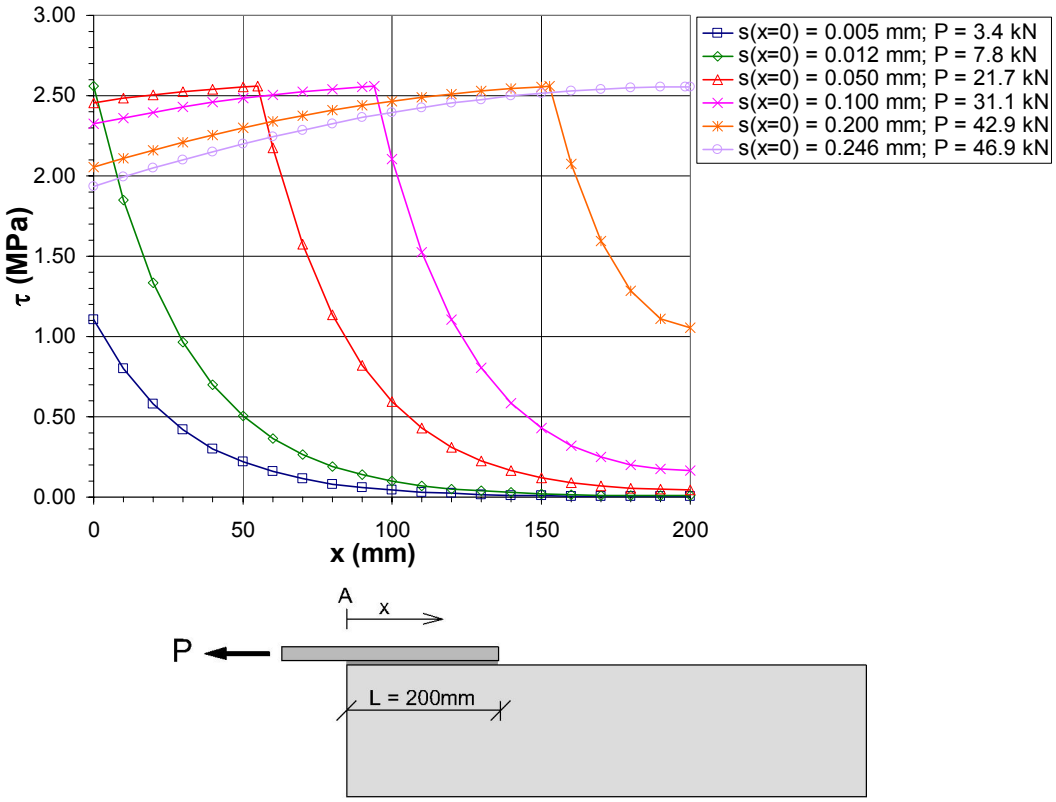

Figure 3.40. Shear stress distribution during Stages 1 and 2a depending on the slip value at $x = 0$.

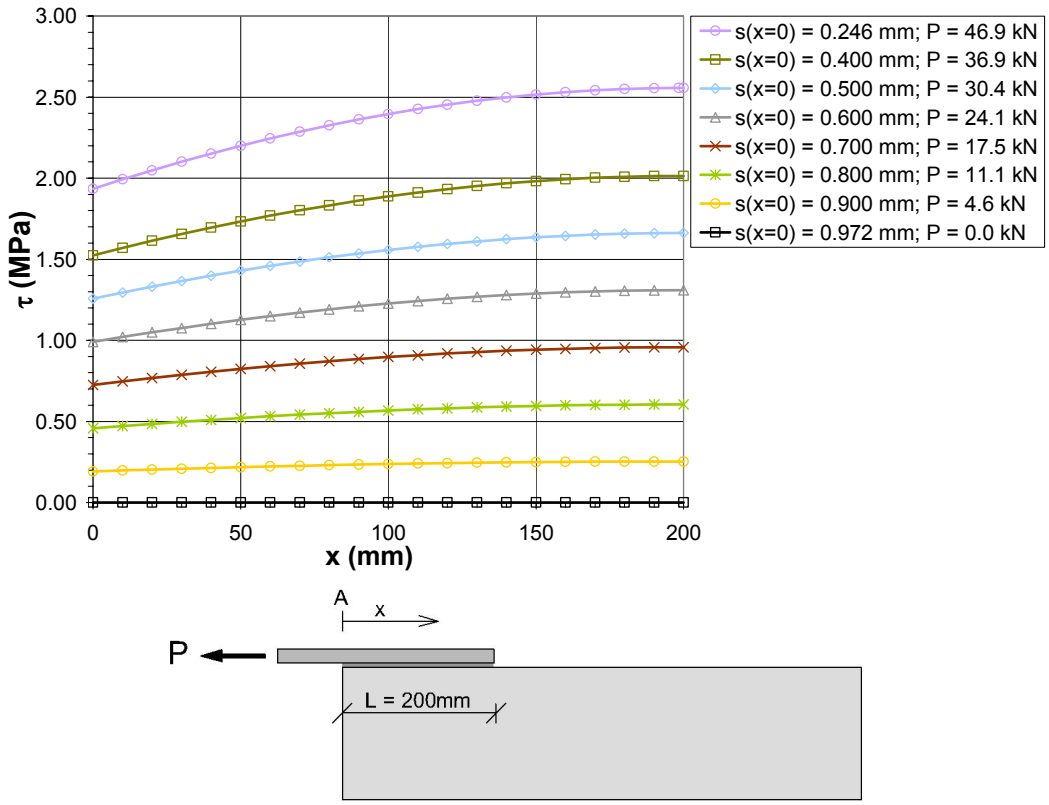

Figure 3.41. Shear stress distribution during Stages 2b depending on the slip value at $x = 0$.

The laminate tensile stress distribution is given in Figure 3.42 for Stages 1 and 2a. The same trends observed for long laminates can be seen in this case. The maximum tensile stress, 336.0 *MPa* is reached at the loaded laminate end when Stage 2b starts.

Figure 3.43 shows the laminate tensile stress during Stage 2b. The tensile stress at the loaded end decreases, as well as the transferred force. As previously mentioned, Stage 2b is only possible when controlling the slip and not the laminate tensile force at the loaded end. At the end of Stage 2b, the laminate completely debonds and there is no tensile stress at any location.

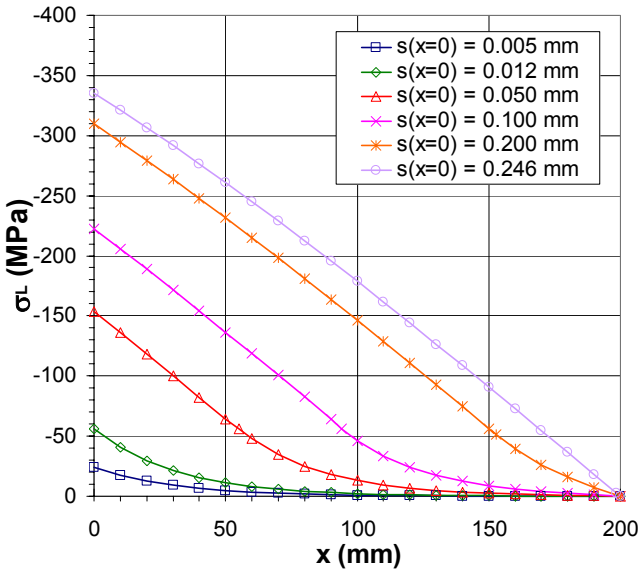

Figure 3.42. Laminate tensile stress distribution during Stage 1 and 2a depending on the slip value at $x = 0$.

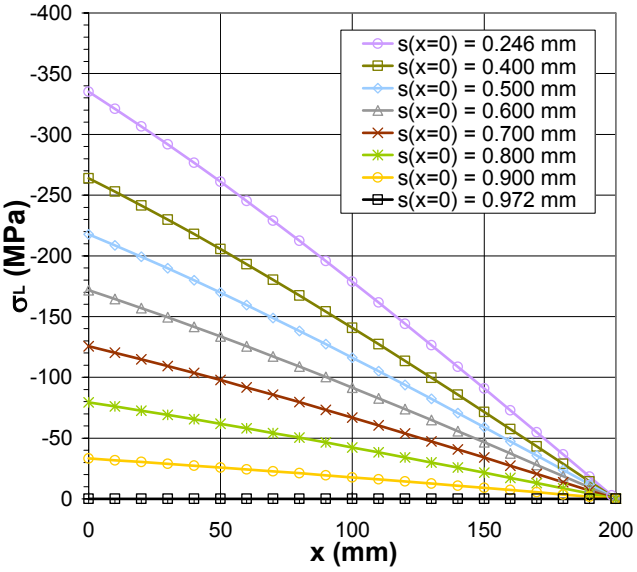

Figure 3.43. Laminate tensile stress distribution during Stage 2b depending on the slip at $x = 0$.

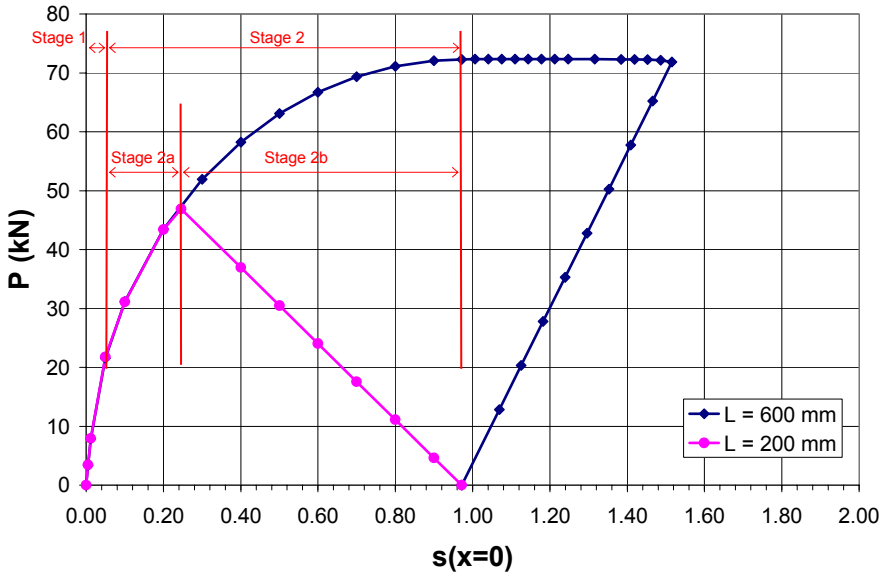

Figure 3.44. Comparison of the transferred force vs. relative sliding at the loaded end of the laminate between L = 600 *mm* and L = 200 *mm*.

Figure 3.44 compares the transferred force between concrete and laminate for the long (600 *mm*) and short (200 *mm*) laminate. Both profiles are very similar up to the point when, in the short laminate, the maximum shear stress reaches the free laminate end. In this case, the transferred force starts to decrease from this point in an almost linear way. The maximum force transferred is much higher in the long bonded length example, 72.2 *kN*, than in the short laminate case, 46.9 *kN*. The maximum force related to equation (3.76) gives the same values as those found by direct integration of the shear stresses along the laminate. For the short laminate, once the maximum force is reached, that is when the maximum shear stress reaches the free laminate end, a load relaxation starts as long as the relative sliding continues to increase. For a long laminate, when τ_{LM} reaches the free laminate end, the transferred force decreases with decreasing values of the relative sliding at $x = 0$.

In Figure 3.45 the relative displacement between the concrete and the external reinforcement during Stage 1, 2a and 2b is shown. It can be appreciated that the sliding decreases from the load application point up to the free laminate end. Once the applied load is 46.9 *kN* or the sliding at the loaded end is equal to 0.246 *mm*, Stage 2b initiates, the complete interface acts in Zone II, and the relative sliding near both laminate ends increases significantly. The relative displacement at the free end of the laminate is different from zero because there is no restriction on its movement. If a bonded or mechanical anchorage was placed at the end of the laminate, the contour conditions would have changed and the sliding at this location would have almost been zero.

Similar to the shear stress distribution, the slope of the plotted lines diminishes as Stage 2b develops. The maximum sliding s_{L0} is reached at the same instant along the complete bonded length.

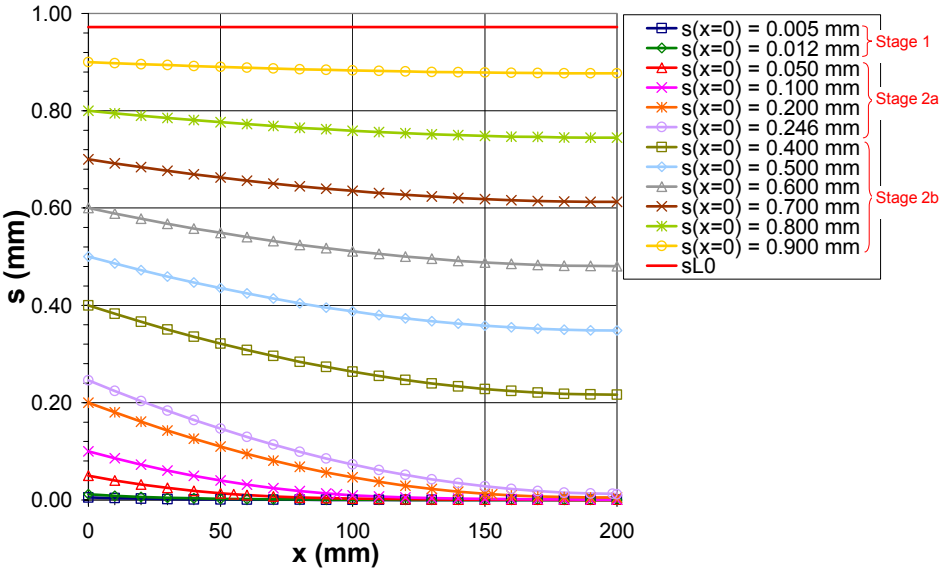

Figure 3.45. Relative displacement between concrete and laminate during Stages 1, 2a, and 2b.

3.9. Verification of the proposed equations using the experimental single/double shear test database

The formulae derived in §3.3 and §3.4 have been verified in terms of maximum transferred force by using the experimental database of single and double shear tests presented in Chapter 2 and detailed in Appendix B. The database consists of 185 shear tests from which a total of 33 tests were excluded: 17 tests because no information about the experimental failure load was available and 16 tests because their mode of failure was by FRP rupture. Therefore, a total of 152 specimens from the database have been studied.

The experimental maximum force obtained during the test has been compared to the theoretical maximum force given by equation (3.76). The ratio between both values indicates the approximation of the theoretical formulae to the experimental results. Ratios (P_{exp}/P_{max}) higher than 1.0 show that the theoretical formulation is conservative and underestimates the response of the strengthened element. This is the case for 73 out of the 152 tests studied.

By using the formulae of §3.3.6, the arithmetic mean of the ratio between experimental and theoretical maximum force is 1.04 with a standard deviation of 0.36. The median is 0.99, similar to the mean, which gives an idea of the homogeneity of the sample. The coefficient of variation, known as the ratio between the mean and the standard deviation, is 34%.

The same statistical analysis was undertaken in distinguishing the material employed in the strengthening of the different samples: Steel, AFRP, CFRP, GFRP. Table 3.5 summarizes the minimum (column 4), mean (column 5), maximum (column 6), median (column 7), standard deviation (column 8) and coefficient of variation (column 9) of the experimental-to-theoretical maximum force ratio. The best results in terms of mean ratio

are for CFRP laminates. However, the standard deviation of 0.37 is probably the highest because of the largest number of samples. As the median value is less than the mean, safety will be evaluated by using the procedure described by Collins (2001), (see the statistical analysis of Chapter 2). Therefore, safety will be characterized by the median value and the coefficient of variation of a fictitious low data set. After evaluating the coefficient of variation of the fictitious low data set, the value for which 99% of the ratios P_{exp}/P_{max} are expected to be exceeded is calculated as shown in column 10 of Table 3.5. The same procedure will be done with a fictitious high data set to calculate the theoretical value for which 99% of the ratios are expected to be lower (column 11).

Table 3.5. Test-to-predicted debonding strength ratios for all plate materials.

Material	Ratio	#	Min	Mean	Max	Med	Std dev	COV	$(P_{exp}/P_{max})_{1\%}$	$(P_{exp}/P_{max})_{99\%}$
(1)	(2)	(3)	(4)	(5)	(6)	(7)	(8)	(9)	(10)	(11)
Total	P_{exp}/P_{max}	152	0.47	1.04	2.89	0.98	0.36	0.34	0.41	2.02
Steel		23	0.59	1.10	1.64	1.04	0.30	0.28	0.46	1.83
AFRP		6	0.72	0.78	0.82	0.78	0.03	0.04	0.70	0.85
CFRP		107	0.47	1.01	2.89	0.93	0.37	0.37	0.43	2.06
GFRP		16	0.73	1.28	2.01	1.24	0.30	0.23	0.72	2.05

To clarify the results presented in Table 3.5, the ratios between the experimental and the theoretical maximum forces as distinguished by FRP or steel reinforcements are presented in Figure 3.46. The calculated percentiles (1, 5 25, 50, 75, 95 and 99) according to Collins are shown in Figure 3.47.

If FRP laminates are examined alone (Table 3.6), the formulae of the previous sections will seem more conservative for wet lay-up FRP laminates than for pultruded laminates. The standard deviation is very similar in both cases.

Table 3.6. Test-to-predicted debonding strength ratios for FRP reinforcements when distinguishing the manufacturing procedure.

Material	Ratio	#	Min	Mean	Max	Med	Std dev	COV	$(P_{exp}/P_{max})_{1\%}$	$(P_{exp}/P_{max})_{99\%}$
(1)	(2)	(3)	(4)	(5)	(6)	(7)	(8)	(9)	(10)	(11)
Total FRP	P_{exp}/P_{max}	129	0.47	1.03	2.89	0.95	0.37	0.35	0.44	2.07
Wet lay-up laminates		105	0.47	1.05	2.89	1.00	0.38	0.36	0.43	2.12
Pultruded laminates		24	0.51	0.93	1.53	0.87	0.30	0.32	0.41	1.73

The "Demerit Points Classification" of Collins (2001) is applied to this model by assigning a mark called "Demerit Point" to various ranges of the ratio P_{exp}/P_{max}. As observed in Table 3.7, the highest percentage of ratios falls in the range of 0.85 and 1.30 which corresponds to appropriate safety (Figure 3.47). In addition, the model presented in §3.3 scores 123 demerit points. This value is similar to the rest of fracture mechanics models summarized in §3.6, with the exception of Van Gemert's which has a score of 222. As a range of magnitude, the empirical models of Tanaka (1996) (referenced by Chen and Teng, 2001) and Hiroyuki and Wu (1997) score 211 and 200, respectively, representing almost twice the score of the fracture mechanics models. Surprisingly, although Maeda's model (1997) comes from a regression of empirical data, it scores 121 due to a lower coefficient of variation.

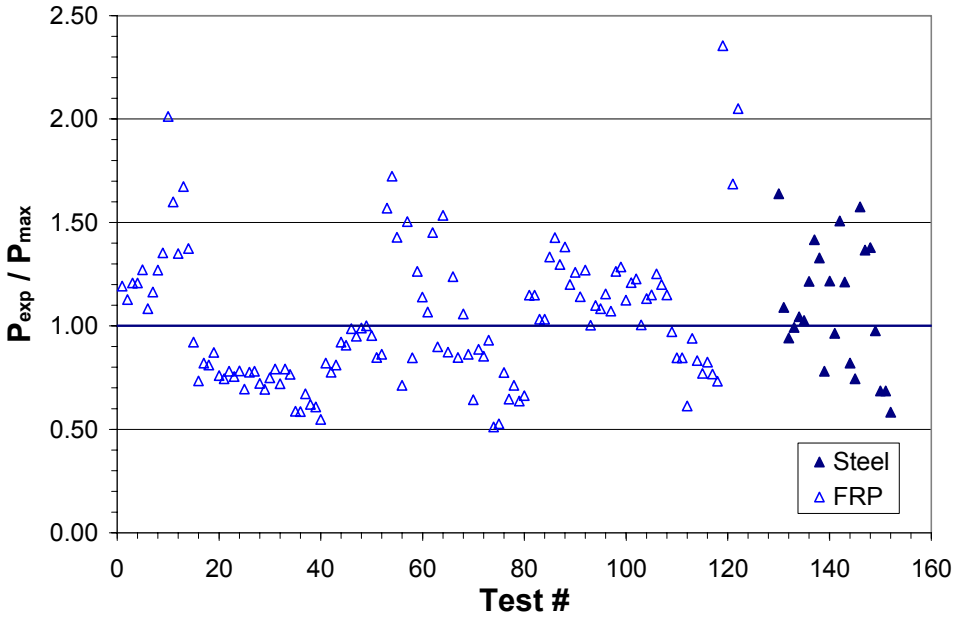

Figure 3.46. Experimental-to-theoretical ratio of maximum transferred force for FRP laminates and steel plates.

When removing those tests without reported adhesive properties (a total of 32 tests of the 152 studied), the demerit point score of the model presented in this chapter decreases to 84 points. In addition, as shown in Figure 3.48, the percentage of ratios with low safety decreases as the percentage of appropriate safety increases.

Table 3.7. Demerit point classification for pure shear specimens failing by laminate peeling-off.

Theoretical model	%	<0.50	0.50-0.65	0.65-0.85	0.85-1.30	1.30-2.00	>2.00	Total Demerit Points
Classification (*)		E.D.	D.	L.S.	A.S.	C.	E.C.	
Demerit Point		10	5	2	0	1	2	
(1)	(2)	(3)	(4)	(5)	(6)	(7)	(8)	(9)
Total	P_{exp}/P_{max}	0.66	7.89	28.95	45.39	14.47	2.63	123
Steel		0.00	4.35	21.74	43.48	30.43	0.00	96
AFRP		0.00	0.00	100.00	0.00	0.00	0.00	200
CFRP		0.93	10.28	29.91	46.73	9.35	2.80	136
GFRP		0.00	0.00	6.25	56.25	31.25	6.25	56

(*) E.D.: Extremely dangerous; D.: Dangerous; L.S.: Low safety; A.S.: Appropiate safety; C.: Conservative; E.C.: Extremely conservative

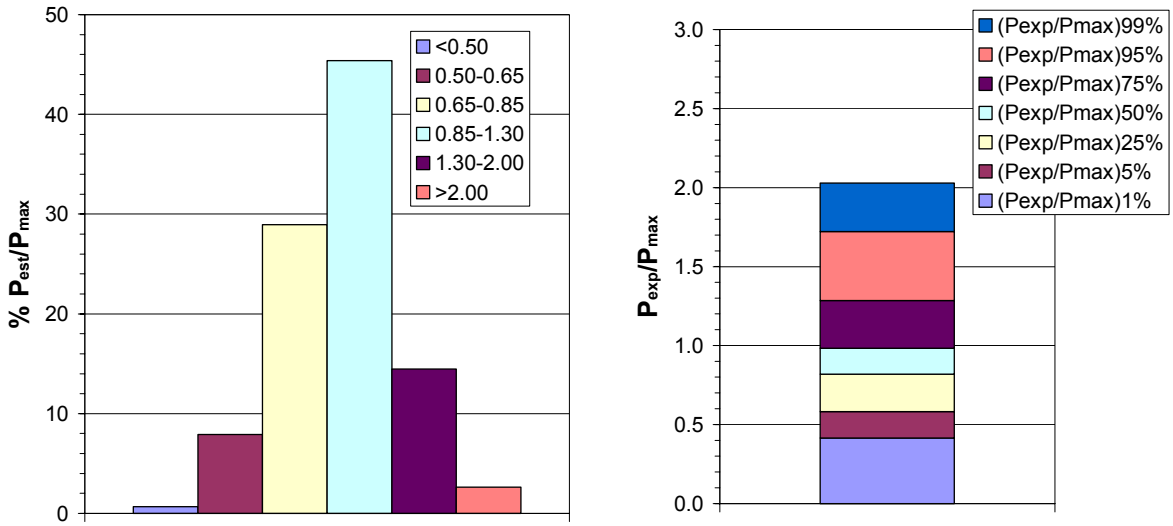

Figure 3.47. Percentages of ratios according to the Demerit Point Classification. Percentiles for the experimental-to-theoretical ratios according to Collins.

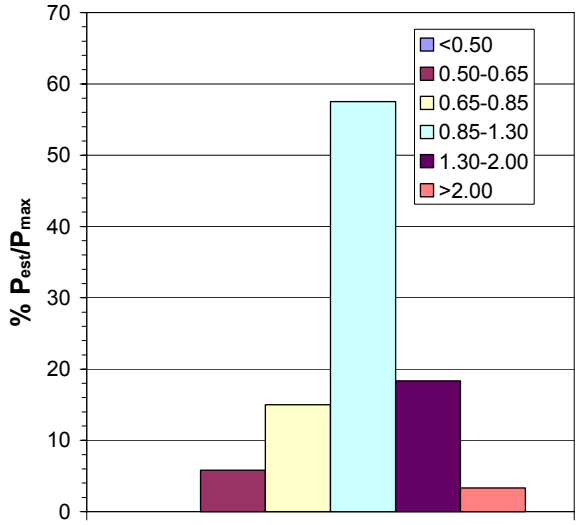

Figure 3.48. Percentages of ratios according to the Demerit Point Classification when removing the tests where adhesive properties were not reported.